UNIVERSIDADE DE LISBOA
FACULDADE DE CIÊNCIAS
DEPARTAMENTO DE FÍSICA

Inclusion of biology in treatment planning for proton therapy

André Lourenço Gonçalves

Mestrado Integrado em Engenharia Biomédica e Biofísica
Perfil de Radiação em Diagnóstico e Terapia

Dissertação orientada por:
Ben Heijmen
Luís Peralta

2017

Acknowledgements

The work for writing this dissertation was done at the Erasmus Medical Centre – Cancer Institute, while integrated in the Radiation Oncology Department in Rotterdam, the Netherlands. I would very much like to thank all the kind, welcoming people I met there during my stay.

Special thanks go to my supervisor Ben Heijmen, and my daily supervisor Steven Habraken, with whom I had very fruitful meetings and interesting debate and banter, and to my home supervisor, Luís Peralta who was supportive and helpful.

I also want to express my deep gratitude to my office colleagues and friends Buddi Sharfo and Rik Bijman, who taught me many things of Dutch culture and language, and who I constantly pestered and distracted with tea.

To all other friends I made: Alba, Amit, Bas, Dominique, Wendy, Thomas, Lovisa, Rens, Thyrza, Yibing, Wendy, Emma, Jordi, Jorris, Carlijn, Patrícia, Xander. Thanks for everything, it was great fun.

Many thanks to my friends from Portugal, who kept in touch through the internet, making the times even more pleasant. Thanks to João, Mariana, Filipa, Afonso, Mafalda, Sara and Bruno, with whom plans always fall apart. Also thank you Iara, Filipe, Francisco, Inês and Joana, for meeting with me in the Netherlands and sharing a fun evening.

Last, but certainly not the least, I want to give a huge thank you to all my family, for the visit, and for the support on every step of the journey, from the first stumble to the last stride. To my parents, without whom I could not even think of going and who support in every possible way; my aunt Mitu and uncle Pedro who are always powerful support and great motivators; to my brother Miguel, of whom I'm so proud, and together with my cousin Diogo kept me company for hours on end and always helped me laugh anything away; to my cousin Francisco, for whom I made a flash visit; to my grandparents who counted the days in reverse while I was gone; and to my other relatives; my biggest thank you. This work would literally be nothing without you.

Resumo

As doenças tumorais são das mais letais em todo o mundo, e são a causa do maior número de mortes após as doenças cardiovasculares. De acordo com a OMS (Organização Mundial de Saúde), estas foram responsáveis por 8,8 milhões de mortes, ou seja, 1 em cada 6 mortes no ano de 2015, e um aumento de 70% da incidência de cancro é esperado num futuro próximo. Em Portugal, o cancro foi responsável por 2516 mortes por milhão de habitantes em 2015, segundo um relatório da DGS (Direção Geral da Saúde).

A radioterapia é uma das modalidades de tratamento prevalentes usadas para o combate ao cancro, a par da quimioterapia e da cirurgia, e que consiste no uso de radiação ionizante de um certo tipo e energia para provocar a destruição de células tumorais. No uso desta modalidade de tratamento, o pretendido é fazer a deposição da radiação no tecido tumoral, enquanto se reduz ao máximo a quantidade de radiação incidente nos tecidos saudáveis circundantes. Deste modo, é possível uma redução ou a completa destruição das células tumorais em crescimento descontrolado, enquanto as funções de tecidos e órgãos adjacentes são preservadas. Para que os efeitos secundários advindos de tratamentos com radiação sejam minorados, é também de grande importância a obtenção de imagens médicas da região de interesse. Estas permitem o delineamento das estruturas próximas ao tecido tumoral, e têm sido, a par das técnicas de tratamento, desenvolvidas nos últimos anos. Entre estas técnicas encontram-se as imagens de CT (*Computerized Tomography*), usadas abundantemente. Técnicas de tratamento são também continuamente desenvolvidas, das quais é exemplo a técnica VMAT (*Volumetric Modulated Arc Therapy*) no tratamento com irradiação usando fotões, em que o tumor é irradiado de vários ângulos, o que permite uma deposição de dose rápida e muito precisa; e o desenvolvimento e uso crescente de irradiação usando partículas carregadas, especificamente iões pesados e protões.

Existem algumas vantagens no uso de protões, e da técnica de IMPT (*Intensity Modulated Proton Therapy*) – modalidade em que, através de planeamento e otimização, a intensidade do feixe usado para o tratamento é alterado para que o perfil de dose coincida com a região do tumor – em relação ao uso de fotões para irradiação, que se prendem com a forma como a sua energia é depositada ao longo do seu percurso, e que culminam nos seus diferentes perfis de deposição de dose. Enquanto os fotões depositam a sua energia maioritariamente a baixas profundidades no tecido que atravessam, levando a uma deposição de dose (energia depositada por unidade de massa) máxima próximo à pele – no caso do uso de EBRT (*External Beam Radiation Therapy*), terapia em que se utiliza radiação produzida no exterior do paciente –, e com um decréscimo contínuo de energia depositada à medida que atravessa tecido. Por outro lado, os protões depositam a sua energia de uma forma abrupta ao chegar a uma certa profundidade num tecido: a deposição é ténue a baixas profundidades e atinge um pico, denominado pico de Bragg, que se encontra localizado a uma profundidade que está intimamente relacionada com a sua energia inicial; e deposita uma grande parte da sua energia numa curta distância. A profundidades superiores àquela em que se localiza o pico de Bragg, o perfil de deposição de dose decai muito rapidamente, com uma deposição residual apenas alguns milímetros após o pico. Devido a estas diferenças, a dose recebida por órgãos e tecidos que se encontrem numa posição proximal à região a irradiar é reduzida quando é usado um feixe de protões, reduzindo a probabilidade de danificar os mesmos; ajustando a energia do feixe de protões, é possível controlar a posição do pico de Bragg em profundidade, o que permite maximizar a dose depositada por cada feixe no tumor; e devido ao rápido decaimento no perfil de deposição de dose na zona distal ao pico de Bragg, os órgãos localizados nestas regiões podem ser mais protegidos.

Por outro lado, a IMPT tem a desvantagem de ser um procedimento mais dispendioso do que a convencional IMRT (*Intensity Modulated Radiation Therapy*), equivalente da IMPT usando fotões, e os aparelhos para o seu uso menos disseminados. Para além disso, o facto de ser um tipo de radiação com propriedades diferentes das dos fotões leva a que o seu efeito em sistemas biológicos seja diferente. Face ao longo e abundantemente estudado uso de fotões, e a estudos conduzidos sobre o efeito de irradiações com feixes de protões sobre culturas celulares, está atualmente estabelecido pelo ICRU (*International Commission of Radiation Units and Measurements*) que para aplicações clínicas, se deve ter em conta que para atingir o mesmo efeito biológico de uma irradiação com fotões de uma certa dose é necessária uma dose de fotões 10% superior, ou seja, que o RBE (*Relative Biological Effectiveness*) de protões tem o valor de 1,1. O RBE pode ser usado para que, dada uma distribuição de dose de protões medida, se possa obter a distribuição de dose de fotões que produz efeitos equivalentes.

O valor recomendado para o RBE é, no entanto, contestado. Em particular, diferentes estudos radiobiológicos reportam valores mais elevados para regiões de maior profundidade em tecido, e o seu aumento de acordo com o do LET_d (*Dose-averaged Linear Energy Transfer*), a energia depositada por unidade de comprimento de trajeto, que é elevado em profundidades próximas ao pico de Bragg e para lá deste. Assim, destas publicações surgem diferentes modelos para o cálculo do RBE baseados no modelo LQ (*Linear-Quadratic*) que usam dados de irradiações de múltiplas linhagens celulares. Estes modelos são baseados nos valores do LET e da dose, que podem ser medidos diretamente. Ainda assim contêm grandes incertezas, que advêm das medições feitas em tecidos biológicos e os efeitos de feixes de protões nos mesmos, particularmente por dependerem do tipo de linhagem celular, da radiossensibilidade de diferentes tecidos, etc. Estes modelos revelam ainda assim que existem diferenças entre o valor atualmente utilizado em procedimentos clínicos e o que é observado experimentalmente, e visto que o valor do RBE é mais alto em maiores profundidades no tecido, é necessário que se tenha em conta este aumento, de especial interesse para os casos em que órgãos saudáveis importantes se encontram imediatamente após o tumor na trajetória do feixe. Aí a dose efetiva D_{RBE} (*RBE-weighted dose*), que pode ser calculada multiplicando a dose física pelo RBE, é mais elevada, e pode levar a que um plano que fosse aceitável baseado na deposição física de dose se torne num plano clinicamente inaceitável por irradiação excessiva dos OAR (*Organs At Risk*).

Devido às incertezas associadas aos modelos do RBE, uma alternativa foi proposta, em que uma versão simplificada do modelo LQ é usada, e que permite relacionar os valores do RBE diretamente com os valores de dose e LET.

No âmbito desta tese, foram implementados modelos analíticos para o RBE, LET e também um modelo unidimensional para a dose, ao longo do eixo de propagação do feixe, usando o *software* MATLAB 2013a. O modelo para a deposição de dose foi útil do ponto de vista da validação da sua implementação, visto ter sido feita de raiz, a partir dum modelo disponível; mas também por permitir o ajuste de parâmetros livres à partida desconhecidos, como a incerteza associada à energia do feixe de protões simulados e um parâmetro de ajustamento entre o cálculo analítico e o obtido do *software* de otimização – ERASMUS iCycle – e cálculo de dose. O modelo para o LET foi também usado como método de validação por comparação com a publicação de origem e para o cálculo de uma distribuição de LET que não é obtida na otimização, e é usada para calcular a distribuição de RBE.

Originalmente, o uso do RBE foi planeado como sendo o alvo de uma nova otimização usando o *software* ERASMUS iCycle, que mediante o fornecimento de uma matriz com a grandeza a otimizar e um ficheiro com restrições e objetivos – *wishlist* – baseadas nos contornos dos órgãos feitos por

especialistas ou por *software* de delineamento sobre a imagem médica do paciente, dá como *output* uma distribuição tão boa quanto possível dessa grandeza sujeita às restrições impostas e objetivos a cumprir. No entanto, uma limitação do algoritmo deste *software* forçou o uso do produto do LET pela dose como grandeza a otimizar. Para além disso, a otimização desta grandeza com relevância biológica foi feita após uma otimização inicial sobre a dose física de protões, visto que esta não deve ser criticamente sacrificada por motivos de aceitação do plano final, num ambiente clínico.

No final, as re-otimizações foram aplicadas em distribuições de dose de fantomas criados por um *software* com geometrias de interesse e com aproximação a casos clínicos. As distribuições geradas foram analisadas através dos DVH (*Dose-Volume Histograms*), que mostram a percentagem do volume de órgãos de interesse a receber uma certa quantidade de dose (e também o produto de dose com LET – LETDVH) recebida, e comparados os valores anteriores e posteriores à re-otimização, com diferentes ângulos de incidência do feixe e com e sem robustez – define se a otimização toma em atenção possíveis erros de posicionamento do paciente e do alvo.

Palavras-chave: Distribuição de dose, Distribuição de LET, IMPT, Otimização biológica da dose, RBE.

Abstract

Intensity Modulated Proton Therapy (IMPT) is particle therapy modality based on the energy deposition profile of protons. Due to the fast energy loss of a proton at a certain depth in tissue, its depth-dose curve has a peak near the end of its range, which depends on its initial energy.

For an IMPT treatment, various sets of proton beams are used to generate successive Bragg peaks, starting from a certain depth and decreasing, in order to fill an irradiation target with an as flat as possible dose deposition plateau – a spread-out Bragg peak (SOBP) –, with each set of beams covering the lateral spread of the target. This leads to a delivery of a conformal dose wash inside that target, while the low dose deposition in the entry region and the almost null one in the exit region allow for a high sparing of healthy tissue.

Protons are particles with different properties to photons used for conventional radiotherapy, so they have a different effect on biological tissues. For that reason, they are given a relative biological effectiveness (RBE) of 1.1, a value which has been shown to differ depending on LET, dose, biological endpoint, etc. RBE is given by the ratio between a dose of a reference radiation (usually a well characterized photon source) and a dose of another kind of radiation, like protons, that produce the same biological endpoint.

In this work, analytical models for dose and linear energy transfer (LET – particle energy loss per unit length) were implemented as a quicker alternative to Monte Carlo (MC) simulations, and to further implement an RBE model, of which the LET is a part of.

Furthermore, this implementation was aimed to be used for biological optimization, but the RBE model is not compatible with the in-house built optimization software ERASMUS iCycle, at the Erasmus MC – Cancer Institute. As an alternative, an optimization on Dose × LET was implemented and applied on a water phantom with some similar to clinical scenario properties.

Implementation of the analytical models worked well when comparing to the original models and worked without errors on a box-shaped water phantom and a head-shaped structure with water density. Optimization also worked after a previous optimization of the physical dose distribution using iCycle.

Keywords: Biological optimization, Dose distribution, Image Modulated Proton Therapy, Linear Energy Transfer, Relative Biological Effectiveness

Contents

List of Figures

List of Tables

List of Abbreviations

µm	micrometer
1D	One-dimensional
3D	Three-dimensional
AP	Anteroposterior
BAO	Beam Angle Optimization
CC	Craniocaudal
cm	mentimetres
CSDA	Continuous Slowing-Down Approximation
CT	Computed Tomography
CTV	Clinical Target Volume
DVH	Dose Volume Histogram
EBRT	External Beam Radiation Therapy
EUD	Equivalent Uniform Dose
g	gram
Gp	giga-protons
GTV	Gross Target Volume
Gy	gray
HN	Head and Neck
ICRU	International Commission of Radiation Units and Measurements
IMPT	Intensity Modulated Proton Therapy
IMRT	Intensity Modulated Radiation Therapy
J	joule
keV	kilo-electron volt
kg	kilogram
LET	Linear Energy Transfer
LETDVH	Dose × Linear Energy Transfer Volume Histogram
Linac	Linear Accelerator
LQ	Linear-Quadratic
LR	Lateral / Left-right
MC	Monte Carlo
MeV	mega-electron volt
MS	Mean square
MV	megavolt
OAR	Organ at Risk

PTV	Planning Target Volume
px	Pixel
RBE	Relative Biological Effectiveness
RS	Range-shifter / Range-shifted
RT	Radiation Therapy
SOBP	Spread-Out Bragg Peak
TPS	Treatment Planning System
VMAT	Volumetric Modulated Arc Therapy

CHAPTER I – Introduction

1.1 – Proton therapy overview

Intensity modulated proton therapy (IMPT) is a particle therapy modality using protons and their properties to deliver an accurate dose to a designated target volume. This modality takes advantage of an important property of proton: their energy deposition profile.

Charged particles, and particularly protons' depth-dose curve (representation of the dose deposition as a function of depth in matter) feature a quick rise followed by a very sharp drop at a certain depth, which depends on the initial energy. This crucial feature of the curve is called the Bragg peak, and happens close to the end of a particle's range in matter, after a slowly rising portion at low depth. The shape of this peak is also changed by the initial energy spread of the generated protons when generating a proton beam, as some variation unavoidable. The resulting beam generated usually from a linear accelerator (linac) is a polychromatic beam, whose Bragg peak is sharper the smaller the spread is [6]. For a complete irradiation of a certain volume, the beam energy must then be changed between different values, for a given direction, for the energy deposition to be done at all the depths needed along the beam axis, generating a spread-out Bragg peak (SOBP) – a Bragg curve originating from a superposition of Bragg peaks of beams with different energies. This is usually done by generating a beam with such an energy that the peak corresponding to it reaches the distal end of the target, and then adding to it beams of lower energies until the proximal end of the target is also covered [7]. Figure 1.1 shows a SOBP, in red, built from the overlapping of pristine (single beam) Bragg peaks, in blue, from protons with different initial energies and therefore, different range. The SOBP extends for a certain range around the prescribed dose (100%), with a steep fall-off. In comparison, the curve of a 10 MV photon is shown, where the shallow peak can be seen, and lower dose delivered to the target area (delimited by the green dot-dashed vertical lines).

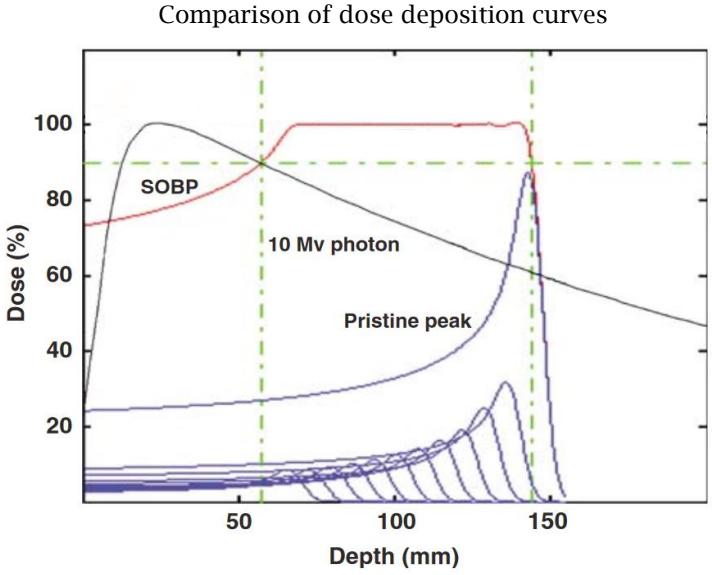

Figure 1.1 – Comparison between depth-dose curves of protons of multiple energies (blue lines) and a 10 MV photon (black line), with the SOBP resulting from the overlap of the pristine proton peaks also shown (red line). The green dot-dashed lines show the SOBP range above 90% desired dose. Adapted from Levin et al., (2005) [7].

The promise behind the use of protons for therapeutic uses, specifically the precise irradiation of tissue and sparing potential has been seen since long ago, being manifested in a paper by Wilson (1946) [8]. Since its inception until today, more than 70 treatment facilities with proton use have been established, with over 40 more under construction, and more still in the planning stage [9].

Proton properties are used clinically, by adjusting beam parameters, and are helpful in delivering a better dose painting profile than what can be achieved with photons. The dose painting inside the whole volume is then made by using enough pencil beams – so named for being narrow, long beams – with varying lateral positioning (pencil beam scanning) as well as depth, which deliver dose spots, adding up to a conformal distribution [10]. Protons' slowly rising depth-dose curve in low depth of tissue, shown as the build-up region in the first stretch of the Bragg curve, contributes to decrease dose in healthy tissue –in stark contrast with photons, which have a high dose deposition at lower depths that decreases with increasing depth – before the target volume, while maximizing the dose inside it, achieving a much better sparing of organs-at-risk (OARs) [11].

1.2 – Target volumes and robustness

IMPT is a technique which requires great accuracy because of the sharp dose delivery profile mentioned above and is therefore quite sensitive to uncertainties in target position [12, 13].

Studies about the interplay between dose profiles generated using images taken previously to the treatment regime, and the variation of patient anatomy before the treatment and between treatment sessions has been and is still studied to understand its effect on tissue surrounding a target volume [14, 15], and these effects are of the utmost importance in cases where the Clinical Target Volume (CTV) – the region receiving, ideally, the most dose – is very close to a major organ, such as, and regarding some of the cases for which proton therapy is best applied, intracranial tumor patients, head and neck (HN) cancer patients, lung cancer patients, and prostate cancer patients. For these cases, the OARs are the ones shown on Table 1.1. such as the optic nerves, optic chiasm, brain stem, etc., in the case of intracranial tumor patients: swallowing muscles, parotid glands, etc., for HN patients; the spinal cord in the case of vertebral bone metastases, the lungs and heart for lung cancer patients and rectum, seminal vesicles, bladder, etc. for prostate cancer patients.

Table 1.1 – List of OARs for different treatment sites on which proton therapy is commonly employed.

Treatment site	**OAR(s)**
Intracranial	Parotid gland, submandibular gland, oral cavity, lips, buccal mucosa, pharyngeal constrictor muscle, supraglottic muscle, glottic area, crico-pharyngeal inlet, cervical esophagus, brachial plexus [16]
Head and Neck	Optic chiasm, cochlea, hippocampus, brainstem, pituitary gland, retina, lacrimal gland, lens [17]
Lung	Lung, bronchial tree, esophagus, spinal cord, ribs and chest wall, brachial plexus [18]
Prostate	Bladder, rectum, right and left femoral heads [19]

Similar issues arise when defining a target volume for treatment with photons [20], although they are handled in a different manner. To account for the risk of irradiating an OAR due to these uncertainties in Intensity Modulated Radiation Therapy (IMRT) and other photon treatment techniques, such as Volumetric Modulated Arc Therapy (VMAT), different planning margins are used, specifically the Planning Target Volume (PTV). The PTV is a contour made around both the tumor volume visible on the planning image – usually a planning Computed Tomography (CT) scan – or perceived by a physician through other means such as palpation or observation by the naked eye – Gross Target Volume (GTV) contour –, as well as the non-visible but estimated disease spread volume around the GTV – CTV contour. This ensures that the PTV contour contains these volumes, and beyond that, it accounts for possible anatomical changes and setup errors in the treatment couch [1]. Figure 1.2 shows a diagram of these planning volumes on the left and the same volumes delineated on a slice of a planning CT scan for a patient with an intracranial tumor.

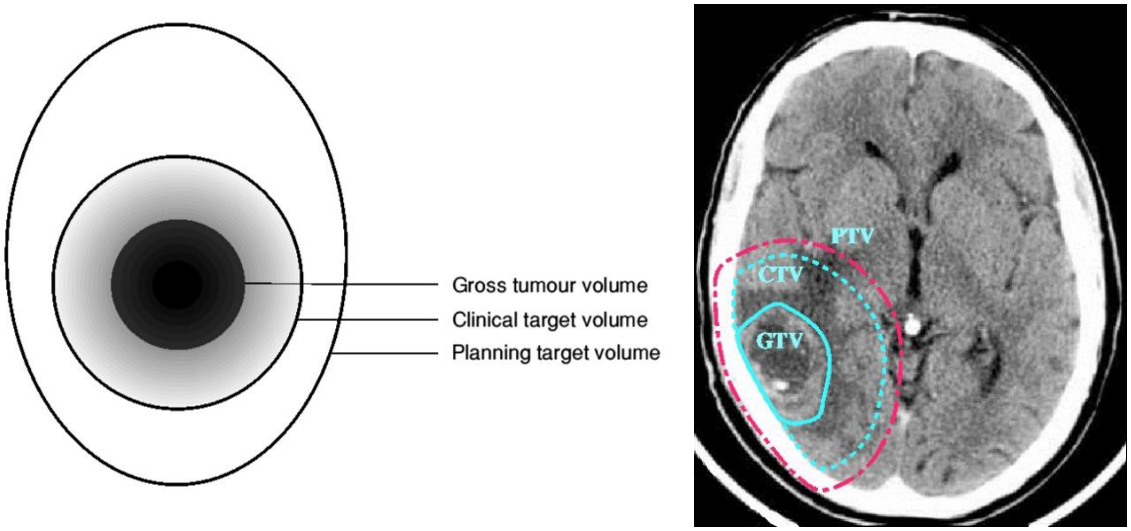

Figure 1.2 – Left: Diagram illustrating the contours usually made for photon therapy planning. Planning Target Volume (PTV) fully contains the Clinical Target Volume (CTV), which in turn fully contains the Gross Target Volume (GTV). Right: Planning CT image of a intracranial tumor patient with the same contours made for a clinical case. Both images adapted from Burnet et al. (2004) [1].

Differently, in IMPT these possible errors are accounted for by requiring a robust optimization in the treatment planning system (TPS), which means the optimization takes several different positioning scenarios of the CTV as possibilities, which include shifts of the original target volume to another position, and errors in the placement or the stance of the patient in the treatment couch, in any of the axes – anteroposterior (AP), craniocaudal (CC) and lateral (LR) – as well as range uncertainties in beam spot (dose hot spot from a single pencil beam) delivery. The dose calculation and optimization is then made with these factors included, meaning the algorithm generates a plan which is acceptable in terms of coverage – volume (or volume percentage) of the CTV receiving usually at least 95% of the prescribed dose – for any of the cases, still maintaining great care for OAR sparing [13, 21].

1.3 – Radiotherapy workflow

The radiotherapy (RT) workflow starts with obtaining a CT scan and identification and delineation of the necessary structures in it, both the ones to spare – the contours of the OARs – and the ones of the target volumes to irradiate. These are identified either by a physician or by an automated

contouring software (nonetheless, it still must be approved by a physician) and exported. A team composed of physicians, medical physicists, radiotherapy technicians, etc. then discusses which technique(s) are most advantageous regarding the case at hand in order to obtain the best outcome, and what fractionation scheme to use for the technique selected. After that, the output from the contouring phase, along with beam entry angles desired and the fractionation scheme selected, are used as input of the TPS to calculate the optimal settings for the beams in order to treat the patient. The fractionation scheme is settled by defining a total desired amount of dose in Gy (gray) to be delivered to the main target volume, and the number of fractions they dose is to be delivered in. Fractionation schemes are decided regarding the disease's type, size, location, among other factors. Choosing the beam characteristics, such as beam energies, the presence or absence of range-shifters (RS) – sheets of a certain material placed on the beam's path, used to reduce the range of a beam (useful to achieve spot delivery in depths corresponding to lower energies than those the accelerator is set to provide, such as in very superficial targets) –, is a process called "plan optimization".

1.4 – ERASMUS iCycle

For this work, a system used at the Erasmus MC Cancer Institute Radiation Oncology department was used. There, the plan optimization is done using a specialized program called ERASMUS iCycle, an in-house developed software created by Sebastiaan Breedveld, in its version for use with proton IMPT. The software optimizes the beam parameters for chosen couch angles and beam directions defined by the user, to deliver the best dose distribution within constraints and requirements included in a wishlist also given as an input [22, 23, 24].

A wishlist is a set of goals organized in order of priority, with the higher ranked elements in the list being optimized towards before the lower ranked ones, and are mostly defined as a function of delivered dose to a certain organ (which is, in the scope of the optimization algorithm, defined by its contour, and thus their importance in treatment planning), and that can set, as an example, the minimum value allowed for the maximum dose voxel inside a structure such as the CTV, as a requirement. The optimization is a mathematical process that assigns relative weights to the objectives to accomplish, each of which has an associated quadratic objective function, and is then subjected to multiple iterations for minimizing the values set in the objectives [25]. It is a multi-criteria problem, since it has multiple constraints and objectives to meet at once, which finally reaches a Pareto-optimal dose delivery plan for fixed beam setups – that is, a plan whose objectives cannot be improved without worsening one or more of the other objectives [26].

After the optimization is done, iCycle's output is sent as input to a dose engine, given to the ERASMUS MC, which simulates the irradiation and produces a three-dimensional (3D) dose matrix – a representation of the deposition of dose inside the patient – which is shaped in such a way that the conditions imposed in the wishlist are met as well as possible, with the top priority ones being optimized first, as calculated in the optimization, using the fluence values also given at the end of the optimization.

1.5 – Project outline

The work done leading to the writing of this dissertation revolves around including biologically relevant data into the optimization and treatment planning: giving physicians a treatment plan including information about the different effects that protons have on biological tissue compared to photons, can improve the quality of plans and help avoid undesirable and unforeseen side-effects.

Information of this nature has an especially important role in proton therapy for tumors located proximally and very close (from the point of view of the gantry/beam) to a sensitive OAR. That is so because the deposition of energy by protons is done near the end of their range. This leads to an increase in Linear Energy Transfer (LET), and consequently in proton Relative Biological Effectiveness (RBE) – seeing as these quantities are directly related – at higher depths in tissue [10]. These effects raise questions about how this quantity is currently used in the clinical context of IMPT. A constant value of RBE = 1.1 for protons is assumed at all depths, as is recommended by the International Commission of Radiation Units & Measurements (ICRU) [27].

One way of taking a more accurate form of the RBE comes from using its definition as a ratio between doses. In this work, RBE is defined as a ratio between a dose of a certain reference radiation (typically a well-characterized radiation type, such as the γ-rays from the ^{60}Co isotope) and a dose of any other radiation type, such as a proton dose, which give the same biological effects [10]. This same biological effect, also called biological endpoint is, in the scope of this work, cell survival. Therefore, what is compared for calculation of the RBE are doses from different radiation types that will produce the same cell survival fraction (percentage of cells that can still divide after receiving a certain amount of dose), since it is an endpoint that directly relates to radiobiological experiments.

To have a calculation of the LET, as it is not measured, and to have a quick way to obtain it, as an alternative to Monte Carlo (MC) calculations, a model was used based on the one present in the papers by Wilkens and Oelfke [3, 28], using analytical functions for the beam fluence on the beam's central axis as well as a model for the stopping power. The models for the fluence and the stopping power are in turn based on the model for dose, using the same quantities, seen in a paper by Bortfeld [2], where the dose deposition curve on the beam axis is modelled analytically. Both the models for the LET and for the dose were implemented for LET calculations as well as for validation.

CHAPTER 2 – LET model, its implementation and validation

2.1 – Model implementation

2.1.1 – Introduction

For LET calculations, two components are needed in general: the proton stopping power and the proton fluence. Analytical models for both quantities are presented by Wilkens and Oelfke [3], and by Bortfeld [2].

Stopping power (S) is a quantity that represents the average loss of energy per unit length ([S] = MeV/cm) along the path of the particles. It was modelled to represent the energy deposition according to the continuous slowing-down approximation (CSDA), with no sudden events or variations of energy loss [29]. It depends on residual range, or energy, which can be used interchangeably, since for protons there is a one-to-one correspondence between (mean) energy and range (the depth of the Bragg peak in water). This relationship can be modelled by a power law, proposed by Bortfeld [2].

The fluence term assumes that, at all depths, the beam energy spectrum is given by a Gaussian distribution due to the randomness of particle interactions, and that the residual range – or energy – of a beam at a given depth along the central axis is such that it allows it to travel between there and its initial range.

An additional term modelling fluence reduction with increasing depth is included in the model, which models the particle loss due to nuclear interactions, linearly depending on depth, and normalized to the initial fluence.

From these components, the one-dimensional (1D) model for the dose-averaged LET along the beam axis can be built, as a ratio between the integration of the stopping power multiplied by a dose kernel and the integration of the dose kernel alone. Since the stopping power is multiplied and divided by a dose, this is called the dose-averaged LET.

The terms previously mentioned are also used to implement the 1D dose model, with an additional term for fluence reduction considered in the paper by Bortfeld [2], where it was first proposed, and which further accounts for fluence reduction from inelastic nuclear interactions, where the incident particle deposits part of its energy locally.

Both models are made assuming the use of a broad beam and then modelling the fluence and stopping power along its central axis, which leads to the possibility of applying them to pencil beams, as is claimed by Wilkens and Oelfke [3].

2.1.2 – Energy-range relationship and stopping power

All models were built with a dependence on depth as opposed to energy, and for that reason, for the dose model it was necessary to build a range-energy relationship. This allowed a translation of a beam's initial mean energy into mean range, and also a meaningful effect of the uncertainties in the beam's energy spectrum on the final result model – the fact that it was an energy uncertainty meant it had to be turned into an equivalent range uncertainty.

This relationship was proposed by Bortfeld [2], in the shape of a power law, as an adaptation of Geiger's rule [30], valid for lower proton energies (up to 10 MeV), which gave the best fit to ICRU data for higher energies (from 10 MeV to 200 MeV). The power law is of the form:

$$R_0 = \alpha E_0^p \tag{2.1}$$

with $p = 1.77$; $\alpha = 2.2 \times 10^{-3}$ cm·MeV^{-p}. R_0, the mean initial range is given in cm and E_0, the mean initial energy in MeV. These values produce a very good fit to ICRU report 49's data as shown in Figure 2.1.

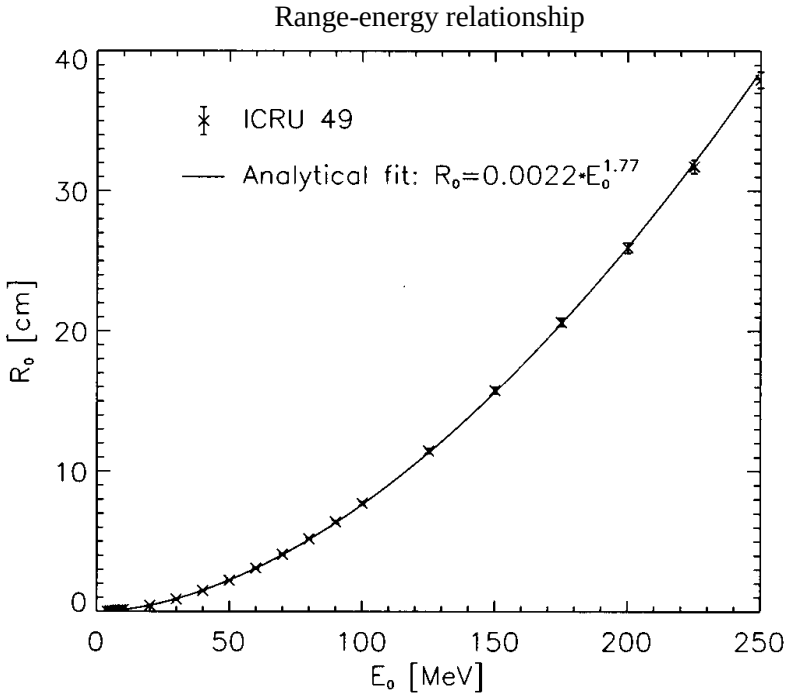

Figure 2.1 – Plot of the range of protons in water as a function of their initial energy. Crosses represent the data points measured by the ICRU, with error bars of ±1.5% and the filled line represents the fit made by Bortfeld and used for the models on this work. Image taken from Bortfeld (1997) [2].

The stopping power model is derived directly from this relation, as it represents the deposition of energy along the particle's path per unit depth. If the remaining energy at a given depth z, given by E(z), is enough for one specific particle to travel the length r (residual range at depth z) between z and R_0 ($r = R_0 - z$), the mean initial range for the beam, the range-energy relationship can be arranged into:

$$E(z) = \left(\frac{R_0 - z}{\alpha}\right)^{1/p} = \left(\frac{r}{\alpha}\right)^{1/p} \tag{2.2}$$

Since stopping power is the derivative of the average energy with respect to the depth z, from equation (2.2), one can obtain:

$$S(z) = -\frac{dE(z)}{dz} = \frac{(R_0 - z)^{1/p - 1}}{p\alpha^{1/p}} \tag{2.3}$$

Where the minus sign is introduced as convention, for a positive stopping power to correspond to an average energy loss.

2.1.3 – Fluence modeling

For the fluence model, the considered contributions are, as explained in the introduction, the Gaussian fluence spectrum and the linear fluence reduction term, normalized to the entrance fluence, Φ_0, which is obtained, for the implementation of the analytical models in this work, from iCycle's optimization results. These are defined in iCycle as beam weights, representing the number of protons in a generated beam – it is saved in the output optimization matrix as a vector, and it stores the number of Giga-protons (10^9 protons – Gp) in each beam.

The Gaussian fluence term that represents the fluence spectrum at a given depth is centered around the proton's residual range r, and the distribution width is given by the standard deviation. In this fluence spectrum model, the standard deviation is a combination of two contributions: one that represents the range straggling for a monoenergetic beam – the uncertainty due to the stochastic nature of particle interactions, dubbed σ_{mono}, responsible for the difference between a single proton's actual range and the beam's initial beam range; and one that comes from the initial energy spread of the beam σ_E, mentioned earlier, since the beam generated in a linac (or any kind of proton accelerator) is not monoenergetic. The latter represents a machine parameter, unknown in this work, as it was a hard-coded value on the dose engine associated with iCycle. Therefore, it was fit to best approach the analytical calculations results to the values output by iCycle and the dose engine. σ_E is given in units of energy (MeV) and must be turned into a length uncertainty σ_r to fit into the range-based model. That is done by putting it through the range-energy relationship as follows [3], and using a simple rearrangement of equation (2.2):

$$\sigma_r = \sigma_E \left(\frac{dr}{dE}\right)_{E = E_0} = \sigma_E \, \alpha \, p \, E_0^{p-1} = \sigma_E \, \alpha^{1/p} \, p \, R_0^{1 - 1/p} \tag{2.4}$$

The calculation involves some manipulations based on the range-energy relationship. The other uncertainty mentioned for the Gaussian modelling due to straggling, σ_{mono}, is given by a power law proposed by Bortfeld that is derived from the MS deviation of the energy at a given depth and an approximation using Bohr's formula [2]. Resulting from this σ_{mono} will be approximated by:

$$\sigma_{mono}^2 \approx \alpha' \frac{p^3 \, \alpha^{2/p}}{3p - 2} R_0^{3 - 2/p} \tag{2.5}$$

where α', like α, is dependent on the stopping material. For water, $\alpha' = 0.087 \text{ MeV}^2 \cdot \text{cm}^{-1}$. Thus, the result for σ_{mono} for water becomes:

$$\sigma_{mono,w} \approx 0.012 \, R_0^{0.935} \tag{2.6}$$

Both contributions are then combined into a single standard deviation σ as a quadratic addition of uncorrelated uncertainties:

$$\sigma = \sqrt{\sigma_r^2 + \sigma_{mono,w}^2} \tag{2.7}$$

which is the final quantity used as a standard deviation for the Gaussian term of the fluence, for calculations in a water medium. Calculations are made by plugging the results from equations (2.4) and (2.6) into (2.7).

Lastly, the linear fluence reduction term, introduced to consider fluence reduction due to nuclear interactions, and relevant for energies above 20 MeV (therapeutic proton energies usually range from 60 MeV to 250 MeV) is approximated by a linear function. After a normalization to the initial fluence Φ_0 yields:

$$\Phi(r) = \Phi_0 \frac{1 + \beta r}{1 + \beta R_0} \tag{2.8}$$

where $\beta = 0.012 \text{ cm}^{-1}$ is the slope for the linear fit to the data present in the paper by Bortfeld – the fact that the value is the same as the coefficient for the $\sigma_{mono,w}$ power law is a coincidence –, and Φ_0 and the denominator are used for normalization.

Finally, the fluence model can be put together from the product of the result given in equation (2.8) and the Gaussian exponential with spread given by the standard deviation in equation (2.7), around beam mean residual range $R_0 - z$, with an additional $1/\sqrt{2\pi}\,\sigma$ term from the Gaussian function, resulting in:

$$\varphi_r(z) = \frac{\Phi_0}{\sqrt{2\pi}\sigma} \frac{1 + \beta r}{1 + \beta R_0} e^{-\frac{(r - (R_0 - z))^2}{2\sigma^2}} \tag{2.9}$$

2.1.4 – LET model

Taking the pieces shown built previously in this chapter, the model for LET can be built. One can directly build a model for what is called the track-averaged LET: a weighting of the stopping power with fluence at the same depth, by making:

$$L_t(z) = \frac{\int_0^\infty \varphi_r(z)\, S(r)\, dr}{\int_0^\infty \varphi_r(z)\, dr} \tag{2.10}$$

where L_t is the track-averaged LET, $\varphi_r(z)$ and $S(r)$ are the fluence and stopping power, respectively.

On the papers by Wilkens and Oelfke [3, 28], and for this work, the LET model used is one for the dose-averaged LET. This is akin to an averaging of the particle's stopping power at a certain depth, weighted by that particle's contribution to the dose at the same depth. From this definition, the model for dose-averaged LET is then:

$$L_d(z) = \frac{\int_0^\infty \varphi_r(z)\, S^2(r)\, dr}{\int_0^\infty \varphi_r(z)\, S(r)\, dr} \tag{2.11}$$

where L_d is the dose-averaged LET, $\varphi_r(z)$ and $S(r)$ represent, in the same way as above, fluence and stopping power. In this definition, the stopping power term in the integral of the numerator squared is due to it being present as part of the dose calculation, as well as by itself, as the quantity being averaged, yielding the result in proper (LET) dimensions.

The components to introduce in the LET model are the fluence as given in equation (2.9), and the stopping power as given in equation (2.3), after being subjected to a regularization. The regularization of the stopping power serves the purpose of removing a mathematical singularity of the model that happens at residual range $r = 0$. Since $p = 1.77 > 1$, then $r^{1/p - 1}$ has negative exponent, and for small values of r, the stopping power would shoot to high values very quickly. Since this does not represent a physical phenomenon, a block-averaging was done to remove this artifact from the analytical

model. It consists on an integral averaging of the stopping power over a small window of width R, called the regularization constant, as is shown next:

$$\overline{S_R}(r) = \frac{1}{R}\int_r^{r+R} S(r')\,dr' = \frac{(r+R)^{1/p} - r^{1/p}}{R\alpha^{1/p}} \tag{2.12}$$

From here on, wherever the LET_d model is concerned, $\overline{S_R}(r)$ as shown in equation (2.12) is taken as the stopping power.

2.1.5 – 1D dose model

For the dose model, the same principles can be used as the ones for the LET model. In fact, the denominator of the dose-averaged LET expression in equation (2.11) is presented in the shape of a dose: a stopping power weighted with a fluence – an integrated product of those quantities [31]. However, in his paper modelling dose [2], Bortfeld introduces an additional contribution to fluence – a reduction term – due to inelastic scattering. This term shows up in the dose model proposed, which is the following for dose deposition in water:

$$\widetilde{D}(z) = -\left(\Phi(z)\,\frac{dE(z)}{dz} + \gamma\frac{d\Phi(z)}{dz}\,E(z)\right) \tag{2.13}$$

This is derived itself from the definition of energetic fluence $\Psi(z) = \Phi(z)\,E(z)$. By differentiating with respect to depth z, and adding, as it was already mentioned, the γ term as an extra fluence-loss modelling term, the following dose kernel is obtained:

$$\widetilde{D}(r) = \Phi_0\,\frac{r^{1/p-1}}{p\alpha^{1/p}}\left(\frac{1+\beta r\,(1+\gamma p)}{1+\beta R_0}\right)\cdot\frac{1}{\sigma\sqrt{2\pi}}\,e^{-\frac{(r-(R_0-z))^2}{2\sigma^2}} \tag{2.14}$$

Besides, this is consistent with the model proposed by Wilkens and Oelfke if the γ parameter is chosen to be zero, and being applied for calculations of dose deposition in water, since the density is $\rho_{water} = 1\ g\cdot cm^{-3}$, an overall multiplication by $1/\rho_{water}$ is omitted, and the final values for dose calculated with this model are in Gy. The full model with consideration for densities other than water can be seen in Bortfeld (1997) [2]. It is tempting, due to the way it was introduced in the model, to interpret the fluence loss pre-factor – fraction between parenthesis including the β parameter in equation (2.14) – including the gamma-term again as an overall fluence loss term. However, it no longer normalizes to 1 in the entrance plane, where $r = R_0$.

For these models, it is important not to forget that since all lengths are expressed in cm for practical convenience, a density of 1 g/cm^3 implies that masses are expressed in g, and energies are expressed in MeV, one must recall that the final (integrated) dose will be given in MeV/g and not in

Gy, so in the end it is required, to make a conversion into SI units, to multiply with a conversion factor $C \approx 1.6022 \times 10^{-10}$ Gy/(MeV·g).

Finally, the form of the dose based on the Bortfeld formulation is, by integrating the kernel in equation (2.14):

$$D = \int_0^{R_0} \tilde{D}_r(z)\, dr = \int_0^{R_0} \frac{r^{1/p - 1}}{p\alpha^{1/p}} \left(\frac{1 + \beta r\,(1 + \gamma p)}{1 + \beta R_0} \right) \cdot \frac{\Phi_0}{\sigma\sqrt{2\pi}}\, e^{-\frac{(r - (R_0 - z))^2}{2\sigma^2}}\, dr \qquad (2.15)$$

In which you can see rearranged, and for dose in water, both the stopping power kernel called S(r) and the fluence kernel called $\varphi_r(z)$ evidently split up. The formula has the form of a dose: Dose = $\int_0^{\infty} \varphi(r)\, S(r)\, dr$. In this case, the upper limit becomes R_0, the maximum range.

2.2 – Validation

2.2.1 – Validating the implementation of the LET model

In Wilkens and Oelfke's work, the optimal value for the regularization parameter previously explained shown to generate the best agreement with MC data was R = 2 μm [3]. As a way of validating the implementation of these quantities, a comparison was made between the implementation done for this work and the figures present in the papers, as the data used to generate those is not available.

One more thing to remark regarding the modelling made in the paper is the fact that there, as the calculations are made analytically, including analytically solving the integrals present in the numerator and denominator of equation (2.11), the resulting formulae include some advanced mathematical functions such as the gamma function and parabolic cylinder functions [3, 2]. As the study and analysis of that kind of function is out of the scope of this work, the integral evaluations were instead evaluated numerically, using MATLAB 2013a and its *integral* function, which automatically computes the integration of an expression using its handle in any interval [32], allowing to avoid implementation of the aforementioned advanced functions. Additionally, it saved the need to do one extra approximation done in the paper which involved approximating the Gaussian function's integral with the rectangle method.

Since this was not done, the LET curves along the beam axis that appear in the comparison do not exactly match the ones present in the paper, although a completely independent check with a Mathematica® script showed that, if the approximation was included, the implementation done for this work and the one by the authors qualitatively (as the data is not available, no quantitative comparison could be made) looked very similar.

Comparison of the results for the LET curves are shown on Figure 2.2. This figure shows the plot of dose-weighted LET as a function of depth in water at a certain range interval. The range focused on is around the depth of the Bragg peak of a E_0 = 160 MeV proton. This energy is equivalent to,

according to the range-energy relationship in equation (2.1) and the parameter values found by Bortfeld (Figure 2.1) [2], an initial range of $R_0 = 17.53$ cm.

Figure 2.2 shows the plots extracted and adapted from the paper by Wilkens and Oelfke [3]: the black dotted line, the three black solid lines labeled with the letters A, B and C, and the series of data points marked by black triangles. The dotted line represents the LET calculated without applying any regularization (R = 0 µm) to stopping power S(r), while the black solid lines represent LET calculated with increasing values for R (R = 1 µm, R = 10 µm, R = 100 µm, from the highest line to the lowest). The triangles represent data obtained from MC simulations, and for that reason, in the paper, the value for R was chosen to best fit this data: R = 2 µm. The colored lines were obtained from the implementation done for this work and overlaid with the original figure (the grid was aligned as well as possible with the length and LET markings) with the same values for R. The pink line (R = 0 µm) matches the paper almost exactly, while the green (R = 1 µm), blue (R = 2 µm), purple (R = 10 µm) and orange (R = 100 µm) lines show an increasing difference for higher depths. The disagreement is due to the previously mentioned avoidance of an approximation via the rectangle method to calculate the integral of the stopping power. Using it would lead to a decrease of LET values close to R_0 when a regularized stopping power is used. Finally, the small colored crosses on top of each colored line come from the same LET calculations made analytically in the Mathematica® software. Those serve as an independent confirmation of the implementation as they were retrieved without applying the final approximation.

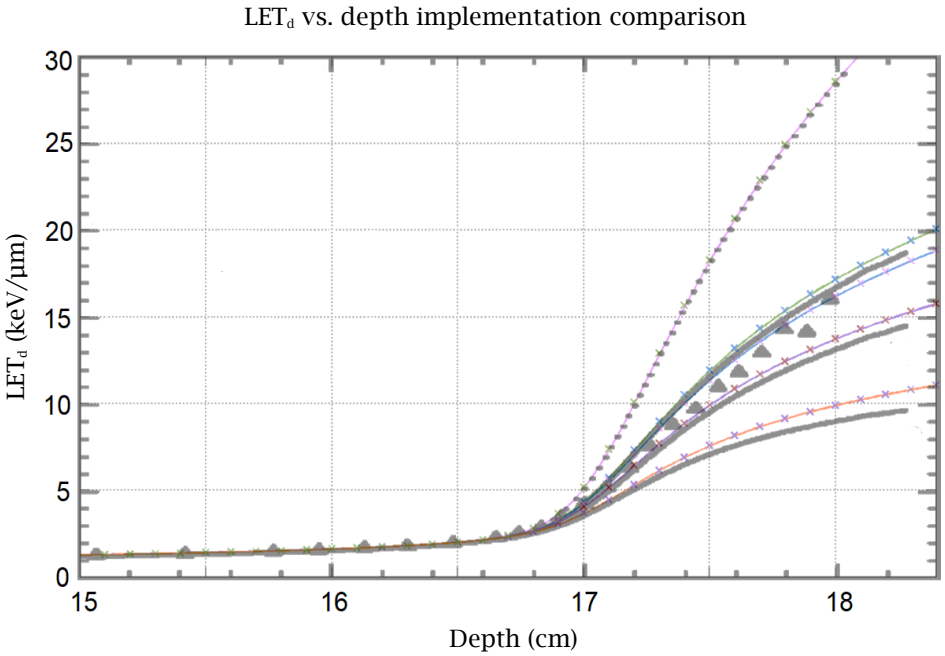

Figure 2.2 – Plot comparison of LET along the beam axis, in water, for a 160 MeV beam energy, between implementation for this work (colored lines), data from the paper of origin (black labeled lines and triangles), and an external check with Mathematica® (colored crosses). See text above for a detailed explanation. Image partly adapted from Wilkens and Oelfke (2003) [3].

Yet another check was done, this time to assure the difference between the paper and the MATLAB implementation lied in the rectangle method approximation. Figure 2.3 shows a comparison between the plots from the paper and data points obtained from Mathematica® with approximation included in both. It becomes clear that the mismatch observed in Figure 2.2 arises from it, as the data points (colored markers) obtained from Mathematica now coincide with the R = 1 µm, 10 µm and 100 µm lines (solid lines) as well as the R = 2 µm Mathematica data set matching very well the Monte Carlo data, as was claimed by Wilkens and Oelfke [3]. The R = 0 µm line was not checked as the approximation only affects LET calculations made with a regularized stopping power.

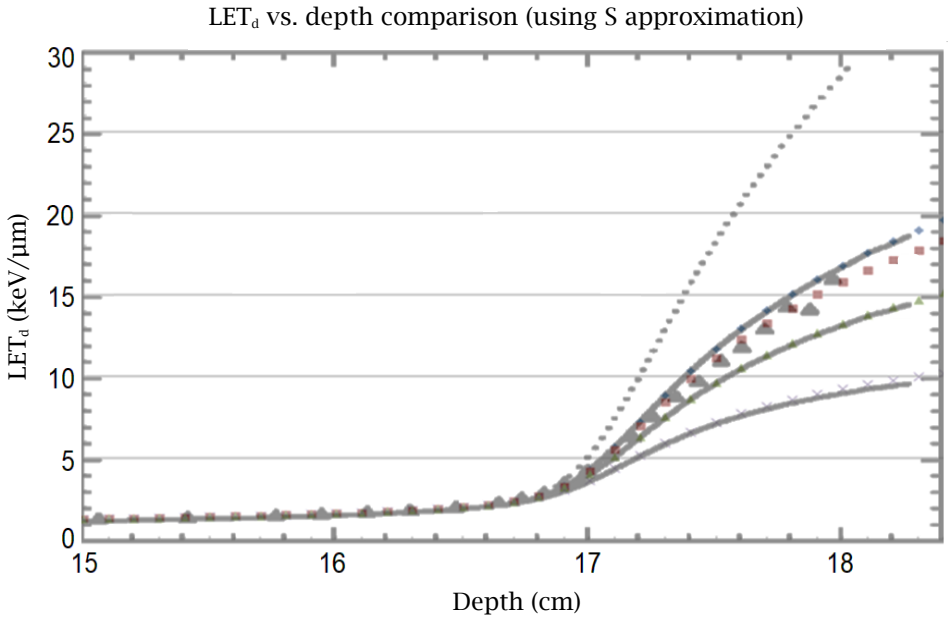

Figure 2.3 – Plot comparison of LET in the same setting as Figure 2.2 using stopping power with approximation. Mathematica® produced data sets (in colored markers) agree very well with plots from the original paper, as expected. See text for further details. Image partly adapted from Wilkens and Oelfke (2003) [3].

From Figure 2.3, it is clear why the regularization value chosen was R = 2 µm. In a context where the additional approximation for S is made, that value seems to be the one to best close in on the MC data produced.

For this work though, the parameter was further changed to fit the MC data set shown in the paper. Since the data values were not available, a visual comparison was once again made in Figure 2.4, using multiple values for R in the LET curves, focusing on values between R = 1 µm (green line) and R = 10 µm (purple line), where the MC values lay. The additional curves are the ones calculated with R = 2 µm (blue line, the same as in Figure 2.1), R = 3 µm (yellow line) and R = 4 µm (gray line). Out of these curves, the one that seems to generate the best agreement is the yellow line, therefore the value for R for the remainder of the calculations of LET will be R = 3 µm.

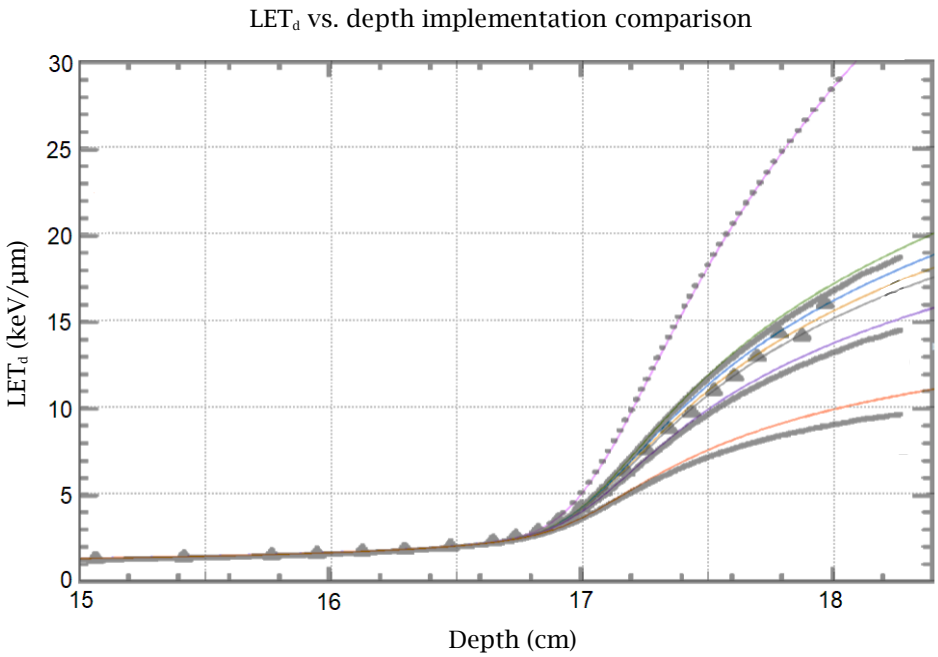

Figure 2.4 – Plot comparison of LET as in Figure 2.2. Using additional values for R in calculation allowed the selection of a value to best fit MC data. R = 3 µm (yellow line) and R = 4 µm (gray line) were the contenders. Visually, the best fit seems to be the former, so that value will be used in further calculations.

2.2.2 – Fitting the LET model to the beam data

2.2.2.1 – iCycle Range-Energy relationship

To turn the analytical formulae presented previously into calculation tools usable in agreement with the iCycle planning system mentioned before, and with its related dose engine, some precautions should be taken, and adjustments made in order to produce consistent and correct results.

The basis upon which the models are built is the range-energy relationship proposed by Bortfeld (1997) [2], explained previously (equation 2.1, Figure 2.1), but for an adequate conversion between the planned locations of beam spots and the energies needed to produce the beams at the correct depths, measurements were made, and the energies required to produce beams at certain ranges were coded into iCycle. That resulted in a range-energy relationship, kept in a look-up table given in the optimization matrix. This set of range-energy data points was taken and fit into a power law, such as the one produced by Bortfeld, and used as the relationship for calculations when using iCycle's data. Figure 2.5 shows the comparison between Bortfeld's power law and the one built using iCycle's table.

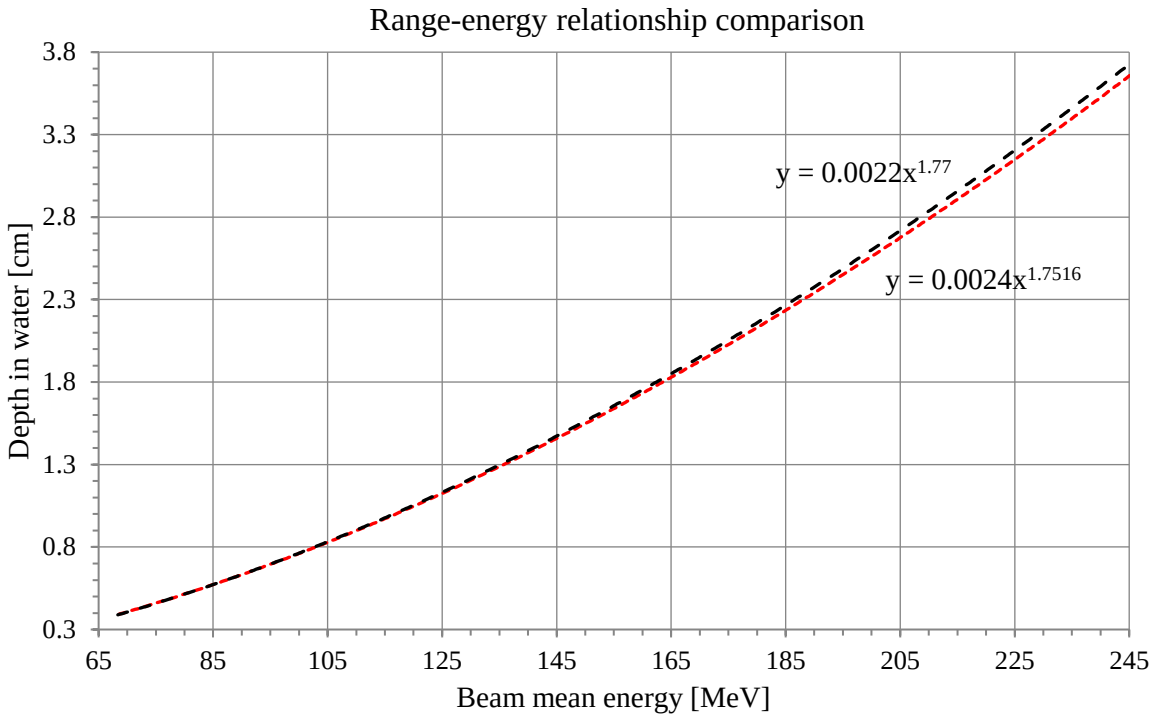

Figure 2.5 – Plot comparing energy-range relationship as given in iCycle's output and from Bortfeld's analytical formula for the same ranges. Data points are not visible due to the abundance (visualization would be cluttered). Power law fits for each are shown instead (red dashed line for iCycle: $y = 0.0024x^{1.7516}$; black dashed line for Bortfeld's: $y = 0.0022x^{1.77}$).

In Figure 2.5 it is visible that for lower energies the power law fits for both data sets are very close to each other, shown by the overlap of the fit. Toward higher energies, the line representing iCycle's relationship becomes slightly lower than the one representing Bortfeld's, meaning that to achieve the same depth in water, the required energy is slightly higher using iCycle's list. This list was made and coded into iCycle and the dose engine associated with it from unknown measurements, so they are assumed to be the ones that best fit any other settings. Although the difference is very small even in the analytical fit parameters, and though the difference is only noticeable for high energies, for calculations done using a range-energy relationship in this work, the iCycle data fit will be used in order to obtain consistent results.

2.2.3 – LET calculation on a water phantom

To compare the calculations made using the slightly adapted model with the process implemented in the optimizer and dose engine, a box-shaped water phantom was created digitally, in an in-house developed software: CASPER. Digital phantoms are useful tools for medical testing, since there is no issue of experimenting on vulnerable patients, and the environment is fully controllable [33, 34]. For this work, it was of crucial importance in test-running the code produced and error corrections, as well as parameter adjustments. The phantom can additionally provide, in a single "patient", many different foreseeable study cases that do not usually show up together.

Being a digital phantom, it was not scanned via CT machine, therefore the mesh of the CT data for it could be chosen and adapted to the needs with relative ease. The dose distribution in Figure 2.6 obtained from iCycle using this phantom together with a wishlist had a slightly higher resolution than 1 mm × 1 mm. The phantom's actual building specifications were 30 cm × 30 cm in the xy-plane, and the slice resolution on the same plane is 309 px × 309 px with a selected resolution of 0.5 mm in depth. The final mesh of dose distributions on this phantom is then 0.97 mm × 0.97 mm × 0.5 mm.

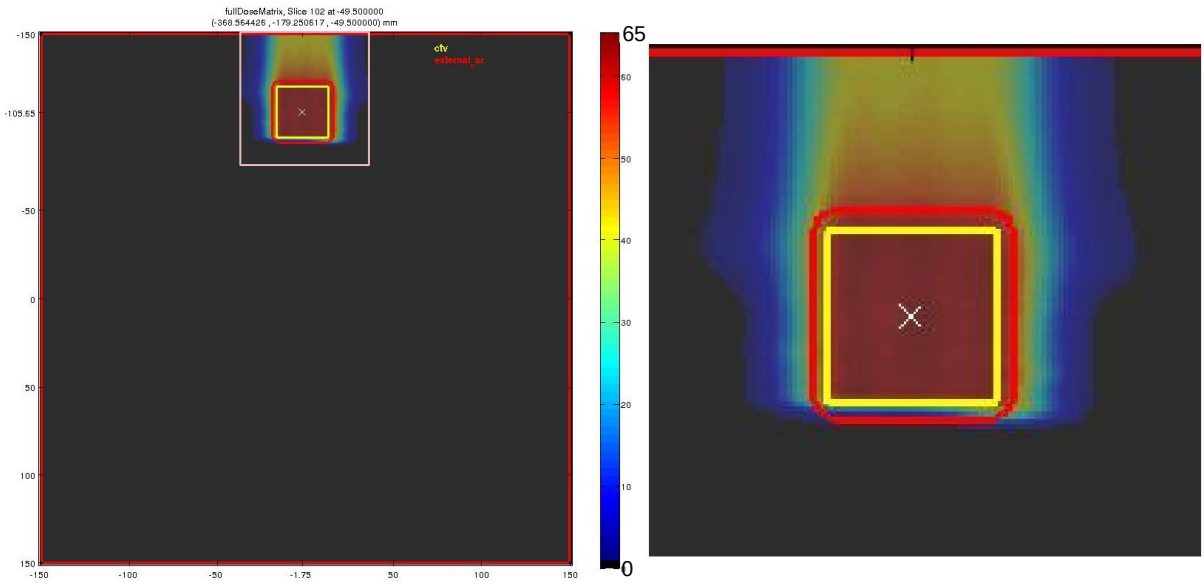

Figure 2.6 – Physical dose distribution on the whole phantom (left) with a single target (yellow contour) and a single beam direction (cranio-caudal). The red contour encompassing the whole phantom except the CTV and a 3 mm margin is defined as OAR. Close-up (right) shows the region inside the light box. Axis values are distance (mm) from the center, and color scale is dose (Gy).

A rather coarse mesh such as described leads to jagged features when plotting the dose generated by the iCycle + dose engine, even if the analytical calculation can be done at arbitrarily short steps (defined by the user), with high precision. Still, to keep computation times low, steps should not be too short, else the gain in time from MC simulations would be lost. Because of the difference in precision, to allow for comparison between both, either the analytical calculation must be made with the same coarseness as the one done by the dose engine, or that the comparison must be done in a rougher way, either by sampling the analytical data at the same depth as the data points available in iCycle's output, or by doing a qualitative comparison, rather than a numerical one. As an additional note: naming iCycle output's resolution coarse is due to it being compared to an adjustable, potentially

higher resolution. The mesh used in dose distribution calculations is standard (or above), and allows for a good enough precision while keeping computation times to a reasonable amount [35].

Figure 2.6 shows a slice belonging to a 3D distribution generated using iCycle with a color wash representing dose delivered to that specific voxel. The whole phantom is water-density, in preparation for the use of the analytical models, but creating different contours as the ones seen: yellow – target volume; red – OAR (includes all the phantom except the target and a small margin) lets the optimizer understand what to irradiate and what not to.

To obtain the distribution shown in Figure 2.6, the wishlist was a simple one, in comparison to clinical ones. Prescribed dose was 60 Gy in 30 fractions, with a constraint on the minimum amount of dose delivered inside the CTV, set to be at least 95% of the prescribed dose (the fractionation scheme for this phantom was 60 Gy in 30 fractions, a usual scheme for head and neck cancer patients), and objectives for minimizing the maximum dose in the CTV to 107% of the prescribed dose (this serves the purpose of avoiding hotspots), minimizing the maximum dose and equivalent uniform dose (EUD) in the rest of the phantom (*external_oar* structure) – EUD is a weighting of the actual delivered dose, which results in the amount of dose that would yield the same effect if delivered uniformly to the selected volume [24].

2.2.3.1 – iCycle to analytical calculation scaling ratio

The previous point on different resolutions also influences how a ratio was calculated between the absolute values of the analytical dose calculation and the absolute values of iCycle output values. This ratio is needed because even using as the initial fluence Φ_0 the number of Gp in a beam in iCycle, the values of the analytical dose obtained did not match the ones generated by the dose engine due to an unknown mismatch.

To calculate the ratio, one can take any number of points from the depth-dose curves obtained with each method (both iCycle + dose engine, and with the analytical model), around the Bragg peak, which is the main feature of the curves that should match, and is also quite convenient to find by coding, as it includes the maximum of the curve. Several different averaging strategies were tried, taking integer multiples of 3 points located proximally to the maximum, and 1 point located distally to it on the curve from iCycle's output, and the corresponding distance points from the analytical model calculations (Figure 2.7).

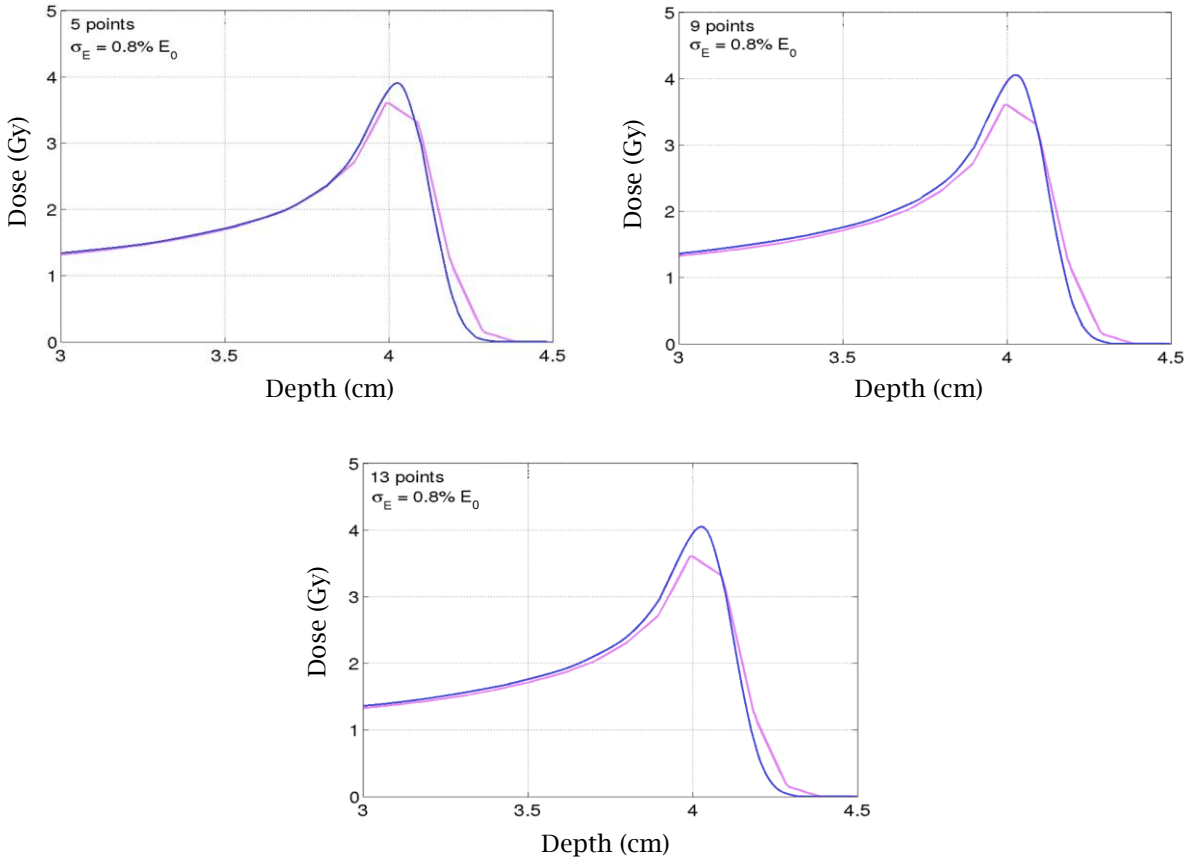

Figure 2.7 – Plots of dose as a function of depth in water, comparing the MATLAB dose (blue) to the iCycle output (pink). Notice labeled near the axis the increasing amounts of points averaged for the ratio calculation around the iCycle peak. All plots are of the same, non-RS beam and using the same initial energy spread (0.8 % of the initial energy E_0).

From this comparison, illustrated in Figure 2.7, the chosen value for number of averaging points was chosen to be 5, as it shows the best agreement between the curves, especially in the build-up region and the fall-off, as the peak itself is expected to be different due to the dose engine calculation being hindered by its lower resolution.

2.2.3.2 – Fitting of σ_E

Besides the ratio calculation, there is also a free parameter in the model, σ_E. It is unknown due to it being a machine parameter and must be chosen to best fit the match between the analytical dose distribution and the one obtained as an iCycle output.

To obtain the optimal value for this parameter, an iCycle plan on the previously mentioned phantom was used, and by comparing the analytically calculated dose, scaled by the ratio explained above, while assuming different values for σ_E (percentages of the beam's initial energy); to the dose generated by iCycle + dose engine, by applying the mean-square (MS) difference method, and also for all beams generated (119 beams) in one plan.

The value for σ_E that achieved the lowest value for the relative MS differences was picked as the optimal one and used for the remaining calculations, as it seemed to be the closest to the actual value for this quantity coded in the dose engine.

The value picked was different for beams that included RS and those that didn't, as the presence of the sheet of material additionally scatters the beam, leading to a wider spatial distribution of the fluence spectrum.

Resulting from an iterative optimization, the values obtained for σ_E were:

- For beams without RS: $\sigma_E = 3.50\ \%$;
- For beams with RS: $\sigma_E = 11.0\ \%$.

These values were chosen as the ones that generated the minimal averaged relative MS differences between the analytically calculated 1D dose profile and the iCycle + dose engine central beam axis for all beams. In Figure 2.8 those are shown for all beams in the plan, with 11 out of the total 119 beams having a RS, generating therefore a smaller sample to choose from. Nonetheless, the σ_E that contained the least average of all beams' relative MS differences was chosen.

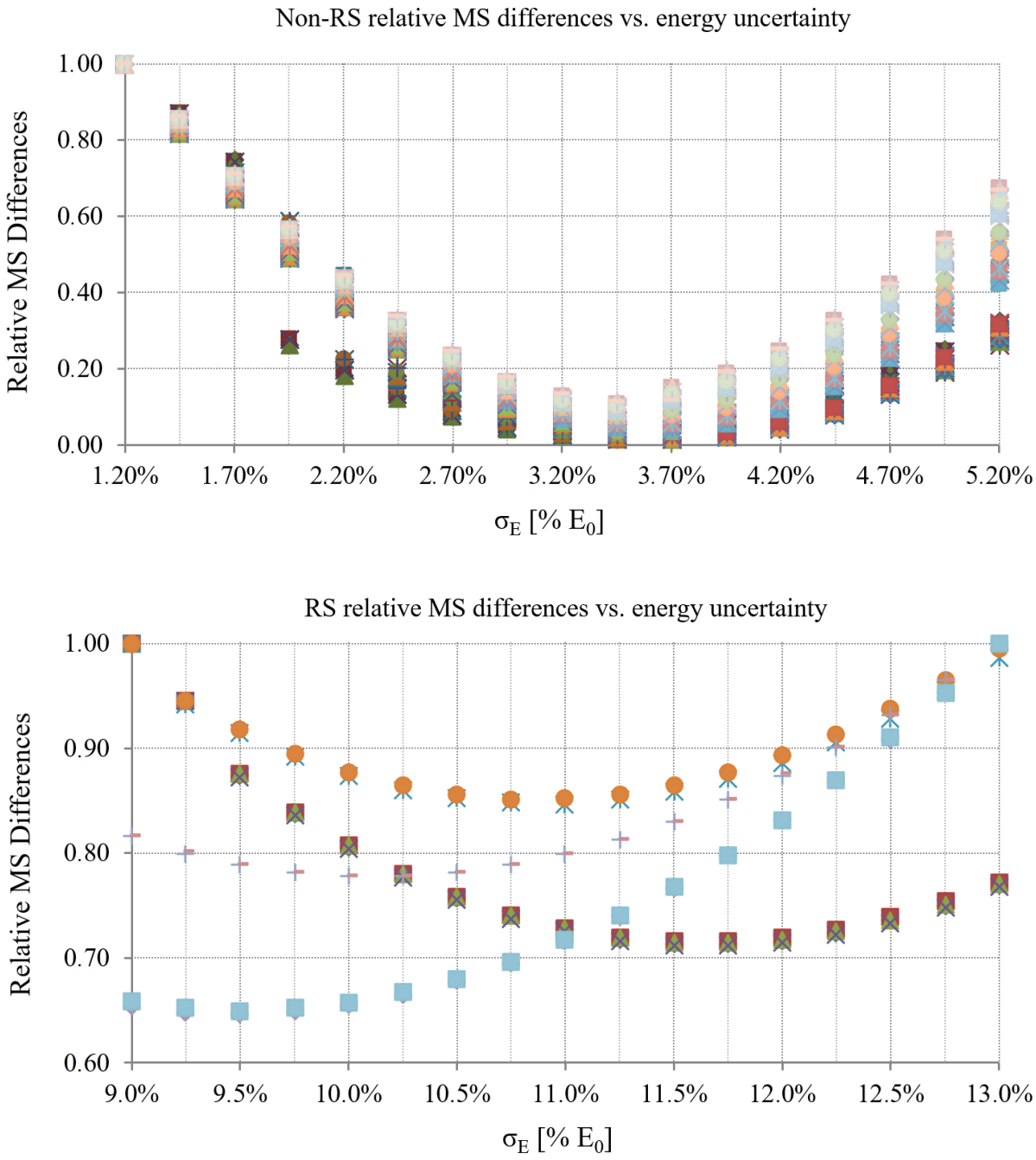

Figure 2.8 – Scatter plots of the relative MS differences between the analytical dose (using the σ_E shown) and iCycle values. Top: Non-RS beams; Bottom: RS beam data. Each set (with equal markers) represents a single beam. The minimum of the averaged values on all σ_E was then picked for both cases.

2.2.4 – Applicability and testing on pre-clinical phantom

Even though the box-shaped phantom was built to encompass some important traits of an actual clinical case such as the target volume being not very far from the skin, as usually happens to tumors treated with IMPT such as HN tumors; the inclusion of RS beams, which may also happen for superficial enough tumors and which causes different amounts of initial scatter due to the presence of the shifting material; and the fact that its target is spread laterally as well as in depth, including different beam ranges and therefore, fluence spread, a test of further applicability was also an aim. To do it, the

calculations for the dose and LET were also done on a CT and structure set of an actual patient, in order to validate it for more complicated structure shapes and more intricate spot distribution setups. The patient was one with a massive intercranial tumor situated in the right lobe of the brain and superimposed with the brainstem.

Because the implementation of the analytical calculations was only valid for water density, the patient's CT data was turned into water density where any other tissue was present (including soft tissues as well as bone, but not air). This resulted in a curved skin surface, as opposed to the smooth and straight surface of the phantom, filled with water in the original shape of the patient's head with air around it. There were still some issues when overriding the inside of the patient's head with water density, as the CT included air cavities and low-density regions, namely the nasal cavity, as it was done manually, using a thresholding method, so some cavities were not filled, leading to some dose overshooting.

Using this patient data set, it was possible to approach a clinical case, and assess that the same implementation of the analytical formulae was applicable in the same form to a case more like a clinical one, with good outcome, as can be seen in Figure 2.9. In it, the dose distribution output by iCycle is shown on the left, with some spillage which was unavoidable in the single beam angle optimization. On the right, a LET distribution showing, as expected, high values towards the distal end of the target and inside the brainstem (OAR), and to the side as well. In regions with lower dose, LET also increases due to being dose averaged.

This exercise was also useful to become aware of and correct for implementation errors when faced with curved entrance surfaces (which is always the case in clinical practice). For this work, adjustments had to be made to the LET implementation when this case was worked on.

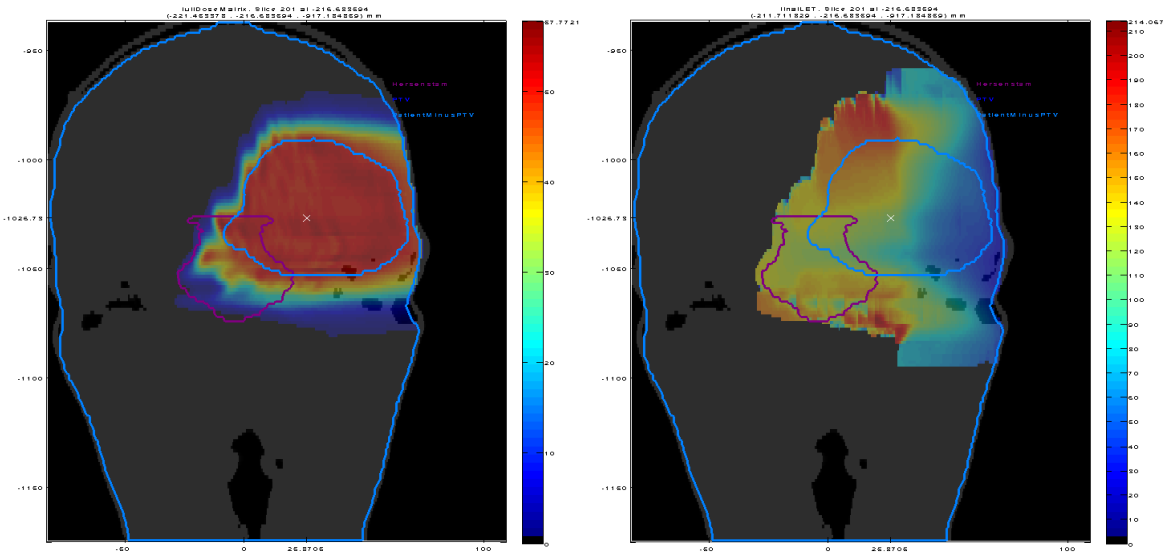

Figure 2.9 – Single beam angle dose distribution (left) in Gy, and LET distribution (right) in keV/µm on the water density-overridden patient CT set. LET distribution is increasing towards the edges despite the dose distribution being fairly well contained in the target volume. On the dose distribution, some overshoot due to visible air pockets can be observed. These stem from the override being done as a mask based on a threshold value for the CT's Hounsfield Units, and leaving therefore some remaining.

CHAPTER 3 – RBE models

3.1 – Model implementation

3.1.1 – Linear-Quadratic model

The LET model explained in the previous chapter is an important physical quantity that has implications upon biological effects. As it is akin to the stopping power, it rises at the end of the path length for charged particles, where the energy loss is faster, since the slowed-down protons at such depth interact more easily with atomic electrons [36]. This higher deposition of energy has an impact on the effect these particles have on the biology of the target, and as such it is included in the model for the RBE [37, 38].

Based on the Linear-Quadratic (LQ) model for cell survival, the RBE model used in this work is proposed by Wedenberg et al. (2013) [37], and it was built for the biological endpoint of cell survival. This is a common endpoint in radiobiological experiments [39], and it is measured by the cell's ability to reproduce after irradiation. The cell survival model gives the survival fraction of a colony as a function of dose delivered to it:

$$S = e^{-\alpha D - \beta D^2} \tag{3.1}$$

where S is the survival fraction, D is the delivered dose, and α ($[\alpha] = Gy^{-1}$) and β ($[\beta] = Gy^{-2}$) are the radio-sensitivity parameters of the model, which denote the response of the tissue to irradiation.

Tissues' responses to irradiation can be characterized into two types. These are either early-responding or late-responding tissue: early-responding tissue is one whose survival ratio decreases after receiving even a small amount of dose; while late-responding tissue can resist to some dose delivered to it, although after a certain threshold the survival ratio decreases for this kind of tissue as well [40].

In the context of the LQ model, late-responding tissue's β parameter is more relevant in its radiation response, compared to the same parameter for early-responding tissue (this means the α/β ratio for late-responding tissues is smaller), leading to a slower decreasing exponential for low received doses, but a sharper drop for increasing delivered dose. On the other hand, early-responding tissue has a comparatively lower β parameter compared to α, and this leads to an immediately decreasing logarithmic linear trend in the survival fraction with increasing dose, with a less pronounced decrease due to the squared term of the exponent in the LQ model [40]. The shape of the curves of survival fraction with respect to dose delivered can be seen in Figure 3.1.

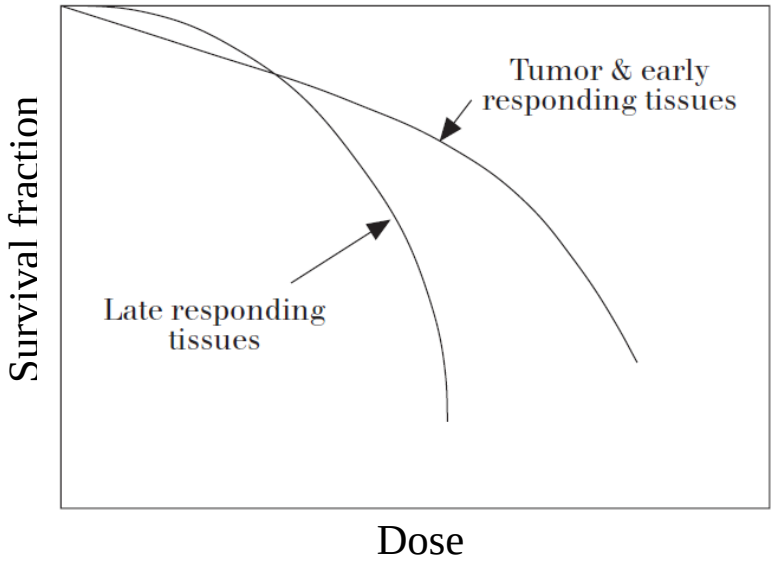

Figure 3.1 – Sketch of the survival fraction of a cell culture (in logarithmic scale) as a function of dose delivered for late- and early-responding tissues. Late-responding: linear component has less impact overall and the quadratic term takes over the dose response; Early-responding (such as tumors): response is immediate for little dose, being dominated by the linear term for lower doses, then it becomes influenced by the quadratic term. Image taken from Padellano (2002) [4].

3.1.2 – RBE definition

RBE is a quantity that is defined as a ratio between doses. On the definition used for this work, RBE is a ratio between a dose of a certain reference radiation (usually from a well-characterized source) and a dose delivered by any other type of radiation, which is in this case a proton dose, that gives the same biological effects [27], meaning, that produces the same percentage of cell survival fraction, since it is a definition directly connected to radiobiological experiments – survival fraction is a quantity that is relatively simple to measure.

As shown above, the LQ model survival ratio (S) is given by equation (3.1).

From the LQ model, one can obtain an expression for this ratio (RBE). Equating the survival ratios for both the reference radiation and the desired radiation type yields an equality between two exponentials with different α and β parameters and delivered dose corresponding to the radiation types being compared.

$$\alpha D + \beta D^2 = \alpha_{ph} D_{ph} + \beta_{ph} D_{ph}^2 \tag{3.2}$$

where the quantities with the subscript "ph" refer to those associated with photons, the reference radiation, and the remaining ones, with no subscript are associated with protons. From this, an expression for the ratio between photon dose and dose of a different radiation type – RBE –, can be obtained by solving the equation (3.2) with respect to photon dose D_{ph}, giving

$$D_{ph} = -\frac{1}{2}\left(\frac{\alpha}{\beta}\right)_{ph} + \sqrt{\frac{1}{4}\left(\frac{\alpha}{\beta}\right)_{ph}^2 + \frac{\alpha}{\beta_{ph}}D + \frac{\beta}{\beta_{ph}}D^2} \quad (3.3)$$

And from equation (3.3), dividing both sides of the equation by proton dose (D), a formula for RBE is obtained:

$$RBE = \frac{D_{ph}}{D} = -\frac{1}{2D}\left(\frac{\alpha}{\beta}\right)_{ph} + \frac{1}{D}\sqrt{\frac{1}{4}\left(\frac{\alpha}{\beta}\right)_{ph}^2 + \frac{\alpha}{\alpha_{ph}}\left(\frac{\alpha}{\beta}\right)_{ph}D + \frac{\beta}{\beta_{ph}}D^2} \quad (3.4)$$

For the model proposed by Wedenberg et al. [37], the ratio between the α parameter for protons and the one for photons is defined as a linear function of dose-averaged LET: $\alpha/\alpha_{ph} = 1 + k \cdot L_d$, where k is a slope parameter which itself depends inversely on $(\alpha/\beta)_{ph}$:

$$k = \frac{q}{(\alpha/\beta)_{ph}} \quad (3.5)$$

In this equation, the value for q is a free parameter, and was selected to be such that it best fit data from radiosensitivity tests. It is independent of L_d, and the value that best fit the data was found to be 0.434 Gy·μm/keV.

The result from equation (3.5) can then be introduced into the RBE formula by substituting in the α/α_{ph} ratio. In this model, as well as in others [41], due to lack of conclusive radiobiological data on the β parameter, it is also assumed that the β parameter for photons is equal to the one for protons: $\beta = \beta_{ph} \Leftrightarrow \beta/\beta_{ph} = 1$.

Taking this into account, and taking equation (3.4), the result is:

$$RBE = -\frac{1}{2D}\left(\frac{\alpha}{\beta}\right)_{ph} + \frac{1}{D}\sqrt{\frac{1}{4}\left(\frac{\alpha}{\beta}\right)_{ph}^2 + \left(q \cdot L_d + \left(\frac{\alpha}{\beta}\right)_{ph}\right)D + D^2} \quad (3.6)$$

where D represents, a proton dose per fraction.

Since the dose as well as LET are 3D distributions [28], this model can give a three-dimensional distribution of RBE as well, of the same size as the dose output given by iCycle. The dose per fraction was, in this work, calculated as a down-scaling of a full dose distribution of a certain prescribed dose to the dose per fraction of the fractionation scheme prescribed. In other words, for a given dose optimization, the result (full dose distribution given at the end of the treatment) was taken and its values

were divided by the number of fractions in the scheme. When calculating RBE with the model, the mathematical operations performed (multiplications, sums, and the square root) are done on each element of the matrix.

CHAPTER 4 – Biological optimization

4.1 – iCycle optimization overview

As stated in Chapter 1, iCycle performs an automated multi-criteria optimization, based on constraints and prioritized objectives, set in the wishlist. The process is done in two phases: the first one goes through the wishlist in decreasing order of priority – starting the optimization by the constraints, and proceeding to objectives of priority 1, then 2, etc. –, until the last objective is reached. When all objectives with a certain order of priority are optimized and their desired values are reached, the optimizer proceeds to the next order while also setting constraints for the previously optimized objectives. This guarantees that the values obtained for those are not lost, but it also means that lower priority objectives are more constrained when their objective functions are being minimized. After this phase, all objectives are either met with a value equal to the set goal, or have a higher value if the constraints in their optimization did not allow the meeting of the goal; the second phase is composed of further minimization of the objectives which could be minimized further than they were in the first phase, as the first phase only pushes the minimization to the set goal values on the wishlist [22, 23].

The optimization results in a collection of beam settings for irradiation of the selected patient, whose CT scan, contour data and specific wishlist are fed to iCycle as an input. The wishlist includes the selected beam directions to irradiate from, as well as couch position and prescribed dose and fractionation scheme for the specific case of the patient in question. These results also include the previously mentioned beam weights (Chapter 2), the amount of Gp in each spot of each beam direction selected in the wishlist.

During the optimization, the way iCycle adapts the expected dose distribution to meet the objectives set is by altering the fluence (or beam-on time – time during which each beam is being used to irradiate the patient –, which is used interchangeably) for the beam spots in each beam. In the end, this means changing the beam weights as they will show up in the output. Because of that, it becomes apparent that, in order for the iterative process to be able to adapt the distribution of a given quantity in a given anatomy, that quantity must depend on the fluence, as is the case for physical dose, so that in one step of the iteration if, as an example, there is one set of spots delivering an amount of localized dose that creates an undesirable hotspot (either outside the target volume, or inside it if one of the aims for the optimization is conformality), the fluences on these are possibly reduced and re-distributed to spots coming from a different direction, to keep an acceptable coverage.

4.2 – Biological data input

4.2.1 – RBE vs. Dose × LET

As stated, for an optimization to be possible with iCycle, the quantity to optimize is required to be dependent on beam weights (conversely, fluence), specifically, that it be linear with respect to beam weights.

Recalling that LET is calculated as a ratio between two quantities, both linearly dependent on the beam's initial fluence, which mutually cancel in the calculation, it becomes apparent that LET is independent of the fluence (it is instead dependent on the energy of protons at a certain depth, conversely, residual range).

Despite LET not having a dependence on beam weights, RBE still gets it, as its calculations (see equation (3.6)) include dose. Unfortunately, the dependence is not linear anymore due to the square root term. This means it is not directly eligible for optimization, although it could be made that way through a linearization around dose values in the dose distribution through a Taylor expansion of the RBE expression shown in Chapter 3. This procedure would add further complexity to the implementation, and especially to computation times, since one evaluation of the expansion would be required for each non-zero voxel of the dose distribution.

Besides, RBE is a quantity whose data measurements are difficult to make with high certainty, and are frequently reported with large error bars [42, 43, 44], adding to it the fact that different patients can have different responses to irradiation even from the same tissue. Opinions regarding its use are divided among authors in the field, some defending that the models based on data with such uncertainty should be used sparingly or avoided altogether [45, 46, 47].

On the other hand, the LET increases have been measured accurately and that is an unambiguously defined and measurable quantity, therefore studies on the effect these increases have on the reaction that tissues show are important, and increased destruction of healthy tissue due to them must be prevented as well as possible.

Due to the points mentioned on the previous paragraphs, an attempt to optimize Dose × LET was made, instead of directly optimizing RBE, avoiding thus the need to apply a linearization on it and spend extra computation time, at the cost of optimizing a quantity that is not physically meaningful, since it is a product of two quantities that, albeit having a meaning themselves, are not immediately relatable.

In the context of a simpler linear model for cell survival, as the one used in a paper by Unkelbach et al. (2016) [5], this quantity can have a more direct relation to how it leads to a biological overdose on high LET regions. In that paper, the model is given by:

$$S = e^{-\alpha D} \tag{4.1}$$

where once again, S represents the survival ratio, D represents dose delivered, and α is a radio-sensitivity parameter which is assumed to have a linear dependence on LET: $\alpha = \alpha_0 (1 + c \cdot L_d)$, such as in the full LQ model. In the same paper, biological dose (B) is defined as:

$$B = -\frac{\log(S)}{\alpha_0} = D (1 + c \cdot L_d) = D + D (c \cdot L_d) \tag{4.2}$$

The result can now be interpreted as follows: the final term shows the biological dose delivered as a sum of the delivered physical dose (D), which can be measured or calculated, and an additional fraction of D, which can be thought of as an effect of LET increase leading to an increase in effective biological dose, B. To adapt this to what is used currently as the standard value for RBE in proton therapy, a RBE = 1.1 would mean $c \cdot L_d = 0.1$ at all points in space. In the scope of a different model, with increasing LET, an increase in biological dose would be observed.

If one wishes to return this rationale to the context of the LQ model, the interpretation is not so straightforward, as in that case, biological dose cannot be separated into factors of physical dose due to the presence of the quadratic term in the model.

One great advantage of using this simplified version is that it is still linear on beam weights, which allows for an optimization using iCycle. This product was therefore selected for optimization instead of RBE. Although it is given in uninterpretable units: [Dose × LET] = Gy·keV/µm – or $J^2/(kg \cdot m)$ in SI units –, and the numerical values it should take are not known, nor are the values to aim for in optimization, it poses a simplification of the implementation, as the "ingredients" used in it (equation (4.2)) are all readily available. Additionally, the results shown in paper by Unkelbach et al. (2016) [5] are promising and represent a middle-ground between solely optimizing on physical dose and optimizing on RBE with large uncertainties. Figure 4.1 shows an optimization example taken from the original paper on how LET-induced additional biological dose (bottom row) was reduced in the brainstem and optic nerve (OARs) while mostly keeping the original physical dose distribution (top row). Also noteworthy is the extra entry dose deposited from the beam entering on the left side (possibly the optimizer's way of reducing spots with ranges very close to the OARs coming from the right side beam, which would deliver high LET to those).

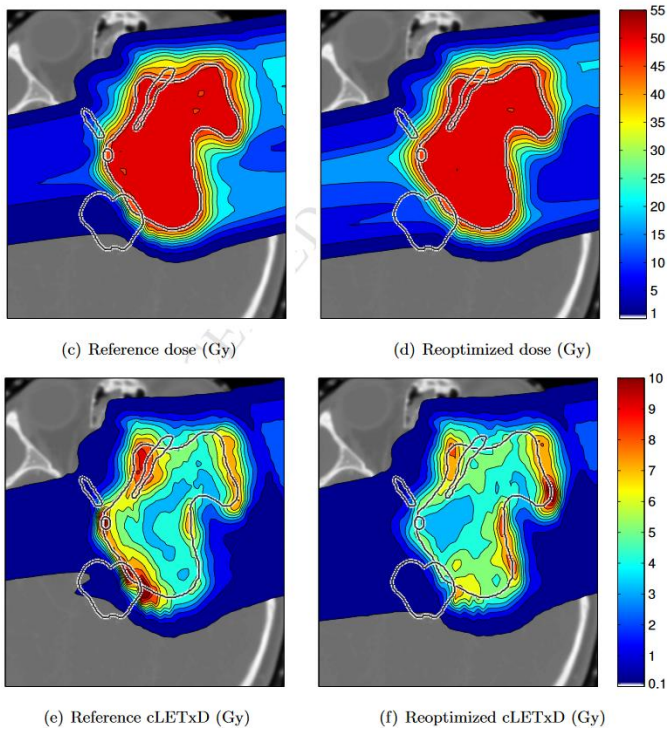

Figure 4.1 – Physical dose (top row) and high-LET induced extra dose (bottom row): before (left column) and after (right column) re-optimization using LET × Dose objectives. Notice the reduction of additional dose to the OARs in the lower right image as compared to the lower left, and the maintenance of coverage and conformality in physical dose to the target. Image taken from Unkelbach et al. (2016) [5].

4.2.2 – Data formatting

To be able to feed the matrix into a pre-existing software requires that the Dose × LET data obtained from the calculations be shaped and prepared for it, so it can be recognized. Usually, iCycle handles formatting of a given matrix by itself, but as biological optimization is not yet included in the main software, some preparation had to be made.

iCycle uses an optimization based on the sampled values from certain voxels inside a contoured region of interest. Sampling is random but it is done to save on memory consumption. Since the sampled voxels must be known to be able to feed the Dose × LET into it, a previous optimization is run so the voxels are selected.

The sampled voxels for dose optimization are the same ones that will be checked when optimizing on Dose × LET. Besides, the beam directions and senses are the same as the ones used in dose optimization, as beam angle optimization was not performed in any step, so the structure of the LET and Dose × LET matrices is compatible with that required by the optimizer.

It is not enough to give the optimizer the full distribution though. The distribution of each spot from each beam direction is required in the first instance, and from this the values of the quantity to be optimized on the sampled points of each region of interest are collected. This is the matrix that iCycle can actually use, and it is a collection of the values of the quantity to optimize on the sampled voxels for each different spot.

4.3 – Re-optimization

After collecting all the one-dimensional data from the analytical calculations of LET and applying the results to obtain a 3D distribution, the optimization must be re-done. For optimization on Dose × LET, a new objective was added to the previous wishlist in the lowest priority possible – at least one priority level below the lowest priority objective present on the original wishlist.

As the purpose of this work was to improve on the LET and Dose × LET distributions obtained after the already established dose distribution optimization, that dose is maintained to the best capacity by not changing the wishlist that led to a satisfactory distribution and only optimizing for Dose × LET after other objectives are met. Thus, one or multiple additional items could be added to the wishlist for reducing its mean value, and since this is not a well-known quantity, the objective values were not known, nor is there a sufficient history of its use to be able to say what the goal is, so the objective was set in order to make the values as low as possible by using a target value of 0 Gy·keV/μm.

For the biological re-optimization phase of this work, the aforementioned phantom was used, although with a different structure set. To make the optimization problem more interesting from the side of the biological effect of the radiation, enhancing what could be gained from this kind of optimization, two structure sets with a 1 cm radius cylindrical OAR and two different disk section target volumes enveloping it were used and the dose optimization was initially made for either (Figure 4.2).

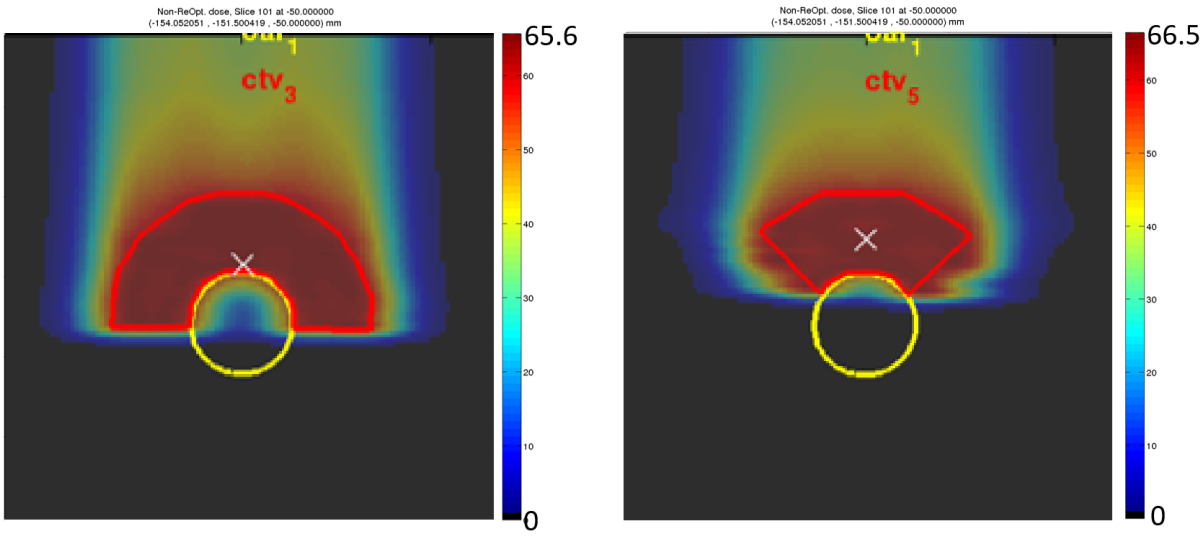

Figure 4.2 – Close-up of dose distribution (physical dose optimization) with a single beam direction for the water phantom with a cylindrical OAR (yellow contour) with a radius of 1 cm, and two different sections of a disk with a large radius of 2 cm and small radius of 1 cm: Left – half disk (180º) section above the OAR, in red; Right – quarter disk (90º) section above the OAR with centered angle. Dose (color wash) in Gy.

After re-optimization, and since the Dose × LET objective was only introduced as the least priority one, the observable visual difference in dose distribution is very small, but is existent nonetheless. To be assured of this, one can now direct their attention to the dose-volume histograms (DVHs) to look for changes in the dose, and to the Dose × LET-volume histograms (LETDVHs) for differences in Dose × LET. A DVH is a clinical and treatment planning tool used for the visualization of 3D data in a compact 2D view. It is convenient since it condenses information of a dose distribution (or Dose × LET in the LETDVHs), by showing in a histogram form which percentage of a volume of interest (vertical axis) received a certain amount of dose (vertical axis). The drawback from using this tool is the loss of positional information. Specifically, just from these histograms it's impossible to directly know about the level of conformality of the distribution [48].

For the analysis of the re-optimization, the focus will be now on the phantom with the structure set containing the smaller target volume (disk phantom).

Using this structure set, the results presented will be for a prescribed dose of 60 Gy, a simple objective list, similar to the one used for the phantom with a square target (with the target volume being now just the section of a disk), but with cases with and without robustness – when the robustness setting was turned on, the setup errors were set to 3 mm (accounts for that much error in the couch and patient positioning) and the range errors to 3 % (accounts for that much error in beam range) –; and cases with a single vertical beam and with 3 beams – one vertical and 2 lateral (left and right).

4.3.1 – Disk phantom

4.3.1.1 – Single beam, robust disabled

For a single vertical beam without any robust optimization, the dose is as seen in Figure 4.2, and the change with optimization is also unnoticeable, although it is confirmed to happen. Differences in the iCycle output's beam weight matrix and the computation of the dose difference are a proof that the optimization runs without errors. A close-up of the difference can be seen in Figure 4.3. It is quite a small difference that stems from the fact that, due to having a very small amount of degrees of freedom, as there is only one beam and no robustness cases.

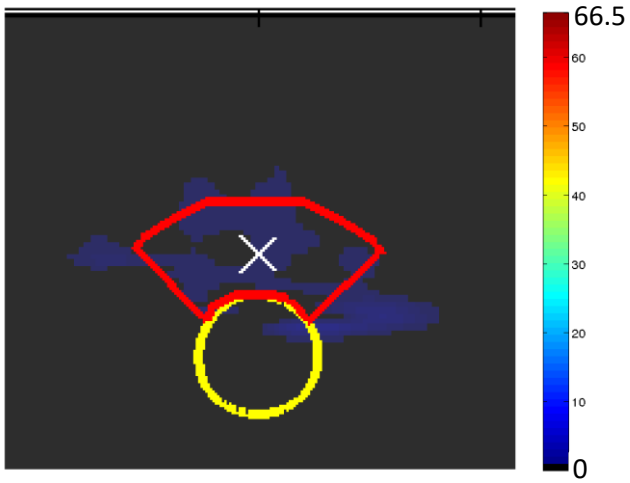

Figure 4.3 – Exemplary slice of the dose difference distribution (color wash — Gy) between physical dose before re-optimization and after. Very low values are shown, but the difference indicates a shuffle in the values of iCycle beam weights (negative values are not shown).

By looking at the DVH. and LETDVH, though, some more information can be obtained. In Figure 4.5, the DVH comparing dose delivery in the OAR (*oar_1*, blue lines) and in the CTV (*ctv_5*, green lines) before re-optimization (solid lines) and after (dashed lines) can be seen. By definition, all DVH lines start at the top left corner, because every bit of volume of any structure received at least 0 Gy. In this figure, it is possible to see that despite the limitations of this setup, before re-optimization, under 35 % of the OAR received any amount of dose. On the other hand, only about 85 % of the CTV volume received the prescribed 60 Gy, and a bit under 95 % received 95 % of the prescribed dose (57 Gy). Comparing the curves between optimizations shows a slight overdose in the CTV after biological re-optimization which afforded a marginal improvement in OAR dose. These effects may be explained by the decrease in fluence of the spots placed near the OAR (at the distal edge of the CTV) and shift to beams in a more proximal or lateral position. This seems like a plausible explanation, but the fact that the dose difference is so small does not allow a definitive conclusion.

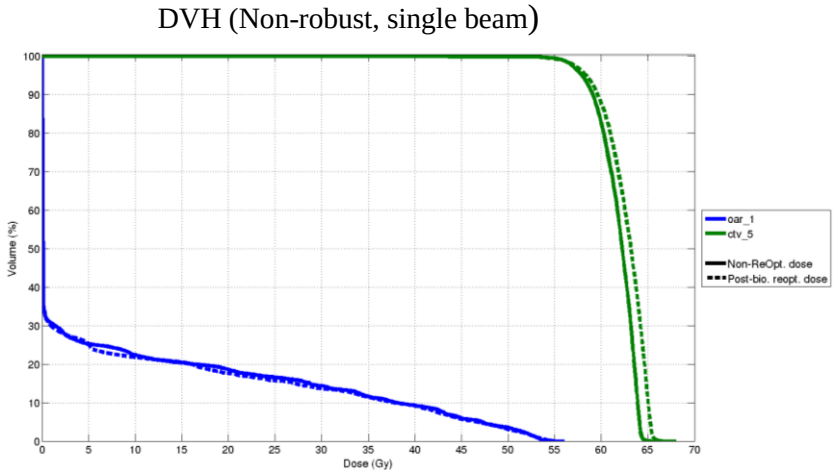

Figure 4.4 – DVH curves of the *oar_1* and *ctv_5* structures (blue and green respectively), comparison between before biological re-optimization (solid lines) and after (dashed lines). Curves for single beam without robustness. Further explanation in the text.

Figure 4.5 compares the LETDVH curves for the same structures before and after re-optimization. In it, the same pattern as seen in the DVH of Figure 4.4 can be seen, and the increase in Dose × LET for the CTV and decrease for the OAR are likely related to those. Following the rationale for the explanation of that figure, the retraction of the beam weights to beams with lower range switched the dose weighting back as well, so less Dose × LET is observed inside the OAR, but more of it in the CTV. One reason for the minor improvement of Dose × LET along the whole value range, with slightly larger improvement in the lower values and even for the very slight increase near the maximum is that the objective added as the biologically relevant one was set to reduce the mean Dose × LET in the OAR, and not the maximum value or any other statistic.

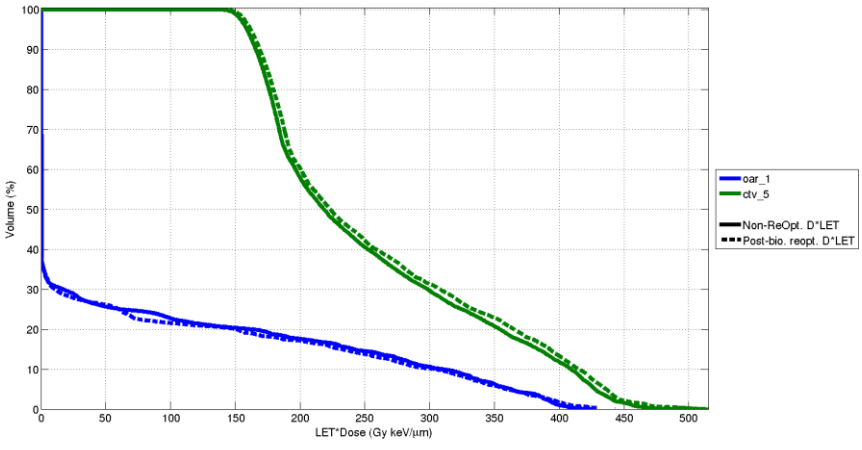

Figure 4.5 – LETDVH curves of the *oar_1* and *ctv_5* structures (blue and green respectively), comparison between before biological re-optimization (solid lines) and after (dashed lines). Curves for single beam without robustness. Further explanation in the text.

4.3.1.2 – Single beam, robustness enabled

Regarding the single beam case with enabled robustness, the analysis is very similar to the one made for the single beam, non-robust case. For this, the dose difference is more noticeable, specially at the lateral borders of the CTV. This happens likely because, having more scenarios in which to adjust the beam weights, while made to keep lower Dose × LET, the optimization algorithm trades some beam fluence on beams that would deliver high LET to the OAR into beams that will improve coverage in every scenario. Therefore, an overdose to CTV is still observed since the dose distribution is "pushed back", and a more marked reduction of OAR dose is seen, as well. Besides, the fact that the robustness errors used are a considerable percentage of the OAR radius might increase these effects.

When analyzing the LETDVH curves, the same pattern as the DVH curves appeared, and the analysis is the as for the single beam, non-robust case.

4.3.1.3 – Triple beam, robustness disabled

When three beams are used instead of one, the optimizer has more freedom in spot placing. An example can be seen in Figure 4.6, which shows the dose deposition of after a 3-beam optimization. The asymmetry in dose deposition from the beam directions is clear. Due to the structures not being completely centered, the preferred direction to irradiate from is the right, as is evidenced by the higher entry dose on that side. On the other hand, it is peculiar that the vertical beam direction having so little path to travel until the target has such a low amount of entry dose, indicating few beams from there.

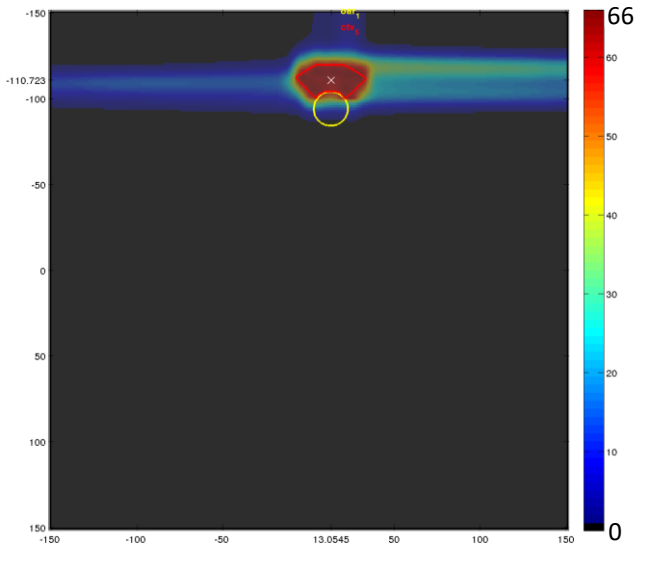

Figure 4.6 – Dose deposition of a 3 bean, non-robust optimization. The green-yellow color at the entry of the beam coming from the right indicates that much more dose is delivered through there than any other direction.

In Figure 4.7 the DVH curves are shown for this case. Despite the additional degrees of freedom in optimization, the improvement in OAR sparing (for both dose and Dose × LET, in the LETDVH) was tiny if any, and the only noteworthy difference was the change from a step-like DVH curve to a smoother curve which might have been caused by a shift of beam weights from the right beam to the left beam, resulting in a more conformal distribution of dose. Nonetheless, the dose to the CTV was

augmented, and the same patterns were observed for the LETDVH. This is, surprisingly, the worst dose distribution so far, even before optimization, regarding OAR sparing. In spite of the availability of other beam directions, including the vertical direction, which yielded much better OAR sparing results in the single beam direction optimizations, it was almost completely disregarded (with only two spots delivered vertically) compared to the lateral beams. Moreover, looking at the beam distribution for each direction, it becomes clear that the beams entering from the right are used to place spots at the leftmost end of the CTV and vice-versa, leaving much entry dose on the CTV.

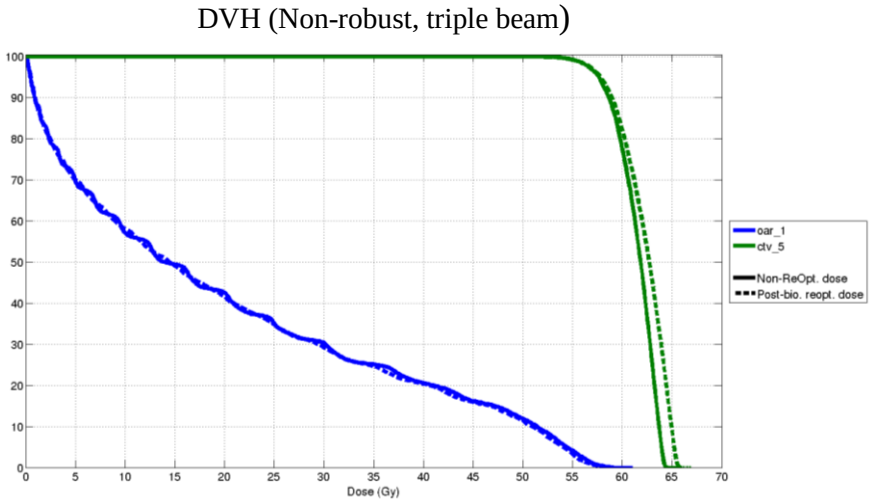

Figure 4.7 – DVH curves of the *oar_1* and *ctv_5* structures (blue and green respectively), comparison between before biological re-optimization (solid lines) and after (dashed lines). Curves for triple beam without robustness. Further explanation in the text.

4.3.1.4 – Triple beam, robustness enabled

The last case investigated for this phantom used 3 beams and the robustness settings already discussed, but the results from this are very similar to the ones for the 3 beams, non-robust case, with even less visible gain on the OAR sparing. In this case, the optimization completely disregarded the vertical beam direction (0 beams) and the target's irradiation was overwhelmingly done from the right.

CHAPTER 5 – Conclusions & future work

Treatment of cancer patients is still a major concern and a still developing field, as cancer is still one of the most prevalent diseases nowadays [49]. Proton therapy is an interesting subject as it has the potential to deliver very accurate treatments and decrease secondary effects such as tissue toxicity or secondary cancer incidence. It is also a challenging field, due to the uncertainty of measurements of radiobiological variables, such as the radio-sensitivity parameters.

Despite the contestation from the proton therapy researchers regarding the use of a variable RBE without sufficient knowledge of the biological quantities that go into modelling it, it is still important to take into account the undisputed fact that LET rises at the end of the beam range. This may still generate issues in the healthy tissue beyond the irradiated target, and should therefore be investigated and addressed as possible.

In this work, a verified implementation of an analytical calculation of LET was shown to be achievable and applicable with relative ease together with a TPS such as ERASMUS iCycle. These analytical functions generate comparable results on the central beam axis with the ones given by the treatment planning system, and are soundly built, so they can be an alternative to lengthy MC simulations, even if not 100 % accurate.

Also, a biologically relevant optimization was run with the established algorithm of ERASMUS iCycle, with positive results, with Dose × LET decreases being observed in the OAR.

These, however, were not fully explored due to time constraints, which prevented the run of extra optimizations using different parameters. Interesting cases include higher-priority biological optimization, even if in a simple phantom case; more complex structure sets and anatomy; different objective types than the minimize mean objective used on all re-optimizations, etc. Outside of the phantom scope, adding tissue heterogeneities and migrating to a heterogeneous version of the analytical models is a must have condition for further development, to achieve applicability in a clinical environment, and gathering of more radiobiological data for improvement of the models. Along with that, patient-specific radio-sensitivity data would be a powerful addition to proton treatment development, if at all possible.

In the near future, application of the analytical LET calculation and possible biological re-optimization on a few patients is being done by Steven Habraken, my daily supervisor and results are expected with great anticipation.

References

[1] N. G. Burnet, S. J. Thomas, K. E. Burton and S. J. Jefferies, "Defining the tumour and target volumes for radiotherapy," *Cancer Imaging,* vol. 4, pp. 153-161, 2004.

[2] T. Bortfeld, "An analytical approximation of the Bragg curve for therapeutic proton beams," *Medical Physics,* vol. 24, pp. 2024-2033, 1997.

[3] J. J. Wilkens and U. Oelfke, "Analytical linear energy transfer calculations for proton therapy," *Medical Physics,* vol. 30, pp. 806-815, 2003.

[4] L. C. Padellano, "Radiation therapy optimization: new strategies for cancer treatment," *Clinical & Translational Oncology,* vol. 4, pp. 49-52, 2002.

[5] J. Unkelbach, P. Botas, D. Giantsoudi, B. Gorissen and H. Paganetti, "Reoptimization of intensity-modulated proton therapy plans based on linear energy transfer," *International Journal of Radiation Oncology*Biology*Physics,* vol. 96, pp. 1097-1106, 2016.

[6] L. Sihver, D. Schardt and T. Kanai, "Depth-Dose Distributions of HIgh-Energy Carbon, Oxygen and Neon Beams in Water," *Japanese Journal of Medical Physics,* vol. 18, pp. 1-21, 1998.

[7] W. P. Levin, H. Kooy, J. S. Loeffler and T. F. DeLaney, "Proton Beam Therapy," *British Journal of Cancer,* vol. 93, pp. 849-854, 2005.

[8] R. R. Wilson, "Radiological Use of Fast Protons," *Radiology,* vol. 47, pp. 487-491, 1946.

[9] Particle Therapy Co-Operative Group, "Particle Therapy Centers," [Online]. Available: https://www.ptcog.ch/index.php/facilities-in-operation. [Accessed 08 17 2017].

[10] F. M. Khan and J. P. Gibbons, The Physics of Radiation Therapy (Edition 5), Philadelphia: Lippincott Williams & Wilkins, 2014, pp. 524-537.

[11] C. T. Lee, S. D. Bilton, R. M. Famiglietti, B. A. Riley, A. Mahajan, E. L. Chang, M. H. Maor, S. Y. Woo, J. D. Cox and A. R. Smith, "Treatment planning with protons for pediatric retinoblastoma, medulloblastoma, and pelvic sarcoma: How do protons compare with other conformal techniques?," *International Journal of Radiation Oncology*Biology*Physics,* vol. 63, pp. 362-372, 2005.

[12] A. J. Lomax, "Intensity modulated proton therapy and its sensitivity to treatment uncertainties 1: the potential effects of calculational uncertainties," *Physics in Medicine & Biology,* vol. 53, pp. 1027-1042, 2008.

[13] D. Pflugfelder, J. J. Wilkens and U. Oelfke, "Worst case optimization: a method to account for uncertainties in the optimization of intensity modulated proton therapy," *Physics in Medicine & Biology,* vol. 53, pp. 1689-17100, 2008.

[14] C. Grassberger, S. Dowdell, A. Lomax, G. Sharp, J. Shackleford, N. Choi, H. Willers and H. Paganetti, "Motion Interplay as a Function of Patient Parameters and Spot Size in Spot Scanning Proton Therapy for Lung Cancer," *International Journal of Radiation Oncology*Biology*Physics,* vol. 86, pp. 380-386, 2013.

[15] J. Seco, D. Robertson, A. Trofimov and H. Paganetti, "Breathing interplay effects during proton beam scanning: simulation and statistical analysis," *Physics in Medicine & Biology,* vol. 54, pp. N283-N294, 2009.

[16] C. L. Brouwer, R. Steenbakkers, J. Bourhis, W. Budach, C. Grau, V. Grégoire, M. van Herk, A. Lee, P. Maingon, C. Nutting, B. O'Sullivan, S. Porceddu, D. Rosenthal, N. Sijstema and J. Langendijk, "CT-based delineation of organs at risk in the head and neck region: DAHANCA, EORTC, GORTEC, HKNPCSG, NCIC CTG, NCRI, NRG Oncology and TROG consensus guidelines," *Radiotherapy and Oncology,* vol. 117, pp. 83-90, 2015.

[17] S. Scoccianti, B. Detti, D. Gadda, D. Greto, I. Furfaro, F. Meacci, G. Simontacchi, L. Di Brina, P. Bonomo, I. Giacomelli, I. Meattini, M. Mangoni, S. Cappelli, S. Cassani, C. Talamonti, L. Bordi and L. Livi, "Organs at risk in the brain and their dose-constraints in adults and in children: A radiation oncologist's guide for delineation in everyday practice," *Radiotherapy and Oncology,* vol. 114, pp. 230-238, 2015.

[18] F.-M. Kong, T. Ritter, D. Quint, S. Senan, L. Gaspar, R. Komaki, C. Hurkmans, R. Timmerman, A. Bezjak, J. Bradley, B. Movsas, L. Marsh, P. Okunieff, H. Choy and W. Curran, "Consideration of dose limits for organs at risk of thoracic radiotherapy: atlas for lung, proximal bronchial tree, esophagus, spinal cord, ribs, and brachial plexus," *Internation Journal on Radiation Oncology*Biology*Physics,* vol. 81, pp. 1442-1457, 2011.

[19] M. Biegala and A. Hydzik, "Analysis of dose distribution in organs at risk in patients with prostate cancer treated with the intensity-modulated radiation therapy and arc technique," *Journal of Medical Physics,* vol. 41, pp. 198-204, 2016.

[20] M. Austin-Seymour, G. T. Y. Chen, J. Rosenman, J. Michalski, K. Lindsley and M. Goitein, "Tumor and target delineation: current research and future challenges," *International Journal on Radiation Oncology*Biology*Physics,* vol. 33, pp. 1041-1052, 1995.

[21] W. Liu, X. Zhang, Y. Li and R. Mohan, "Robust optimization of intensity modulated proton therapy," *Medical Physics,* vol. 39, pp. 1079-1091, 2012.

[22] S. Breedveld, P. R. M. Storchi, P. W. J. Voet and B. J. M. Heijmen, "iCycle: Integrated, multicriterial beam angle, and profile optimization for generation of coplanar and noncoplanar IMRT plans," *Medical Physics,* vol. 39, pp. 951-963, 2012.

[23] S. Breedveld, P. R. M. Storchi, M. Keijzer, A. W. Heemink and B. J. M. Heijmen, "A novel approach to multi-criteria inverse planning for IMRT," *Physics in Medicine and Biology,* vol. 52, pp. 6339-6353, 2007.

[24] G. D. Gala, *A method for automated generation of radiotherapy treatment plans for lung cancer,* Bologna, 2015.

[25] S. Breedveld, P. R. M. Storchi, M. Keijzer and B. J. M. Heijmen, "Fast, multiple optimizations of quadratic dose objective functions in IMRT," *Physics in Medicine and Biology*, vol. 51, pp. 3569-3579, 2006.

[26] The Economic Times, "Pareto's Efficiency," [Online]. Available: http://economictimes.indiatimes.com/definition/paretos-efficiency. [Accessed 9 01 2017].

[27] International Commission of Radiation Units and Measurements, "Prescribing, Recording and Reporting Proton-Beam Therapy (ICRU Report 78)," Oxford University Press, Oxford, 2007.

[28] J. J. Wilkens and U. Oelfke, "Three-dimensional LET calculations for treatment planning of proton therapy," *Zeitschrift für Medizinische Physik*, vol. 14, pp. 41-46, 2004.

[29] National Institute of Standards and Technology, "Appendix: Significance of Calculated Quantities," [Online]. Available: https://physics.nist.gov/PhysRefData/Star/Text/appendix.html. [Accessed 20 11 2016].

[30] R. D. Evans, The Atomic Nucleus, Bombay: Tata McGraw Hill Publishing Company Limited, 1955, pp. 637-653.

[31] E. B. Podgorsak, Radiation Oncology Physics: A Handbook for Teachers and Students, Vienna: International Atomic Energy Agency, 2005, pp. 54-59, 485-504.

[32] The MathWorks, Inc., "Documentation - integral," [Online]. Available: https://www.mathworks.com/help/matlab/ref/integral.html?s_tid=gn_loc_drop. [Accessed 10 11 2016].

[33] Johns Hopkins Medicine, "Digital Phantoms," [Online]. Available: http://www.hopkinsmedicine.org/radiology/research/divisions/medical-imaging-physics/research/projects/imaging-simulation-computer-phantoms.html. [Accessed 18 08 2017].

[34] X. G. Xu and K. F. Eckerman, Handbook of anatomical models for radiation dosimetry, Florida: Taylor & Francis Group, LLC, 2009, pp. 3-7, 618-620, .

[35] S. Webb, The physics of three-dimensional radiation therapy, Bristol: IOP Publishing Ltd., 2001, pp. 27, 28, 38-41, 198-200.

[36] D. Casas, M. D. Barriga-Carrasco, A. A. Andreev, M. Schnürer and R. Morales, "Proton stopping power of different density profile plasmas," *Acta Polytechnica*, vol. 55, pp. 76-80, 2015.

[37] M. Wedenberg, B. K. Lind and B. Hadermark, "A model for the relative biological effectiveness of protons: The tissue specific parameter α/β of photons is a predictor for the sensitivity to LET changes," *Acta Oncologica*, vol. 52, pp. 580-588, 2013.

[38] M. Wedenberg and I. Toma-Dasu, "Disregarding RBE variation in treatment plan comparison may lead to bias in favor of proton plans," *Medical Physics*, vol. 41, pp. 1-8, 2014.

[39] E. Demidenko, "Three endpoints of in vivo tumour radiobiology and their statistical estimation," *International Journal of Radiation Biology,* vol. 86, pp. 164-173, 2010.

[40] E. J. Hall and A. J. Giaccia, Radiobiology for the radiologist (6th edition), Philadelphia: Lippincott Williams & Wilkins, 2006, pp. 37-47, 104-110.

[41] J. J. Wilkens and U. Oelfke, "A phenomenological model for the relative biological effectiveness in therapeutic proton beams," *Physics in Medicine and Biology,* vol. 49, pp. 2811-2825, 2004.

[42] H. Paganetti, A. Niemierko, M. Ancukiewicz, L. E. Gerweck, M. Goitein, J. S. Loeffler and H. D. Suit, "Relative biological effectiveness (RBE) values for proton beam therapy," *International Journal of Radiation Oncology*Physics*Biology,* vol. 53, pp. 407-421, 2002.

[43] H. Paganetti, "Nuclear interactions in proton therapy: dose and relative biological effect distributions originating from primary and secondary particles," *Physics in Medicine and Biology,* vol. 47, pp. 747-764, 2002.

[44] H. Paganetti, "Relative biological effectiveness (RBE) values for proton beam therapy. Variations as a function of biological endpoint, dose, and linear energy transfer," *Physics in Medicine and Biology,* vol. 59, pp. R419-R472, 2014.

[45] H. Paganetti and M. Goitein, "Radiobiological significance of beamline dependent proton energy distributions in a sprea-out Bragg peak," *Medical Physics,* vol. 27, pp. 1119-1126, 2000.

[46] A. Carabe, M. Moteabedd, N. Depauw, J. Schuemann and H. Paganetti, "Range uncertainty in proton therapy due to variable biological effectiveness," *Physics in Medicine and Biology,* vol. 57, pp. 1159-1172, 2012.

[47] A. L. McNamara, J. Schuemann and H. Paganetti, "A phenomenological relative biological effectiveness (RBE) model for proton therapy based on all published in vitro cell survival data," *Physics in Medicine and Biology,* vol. 60, pp. 8399-8416, 2015.

[48] R. E. Drzymala, R. Mohan, L. Brewster, J. Chu, M. Goitein, W. Harms and M. Urie, "Dose-volume histograms," *International Journal of Radiation Oncology*Biology*Physics,* vol. 21, pp. 71-78, 1991.

[49] World Health Organization, "Cancer," [Online]. Available: http://www.who.int/cancer/en/. [Accessed 27 07 2017].